Manuscript 2018-03-03491A

Micro-RNA therapy stimulates endogenous cardiac regeneration after myocardial infarction

Khatia Gabisonia[1#], Giulia Prosdocimo[2#], Giovanni Aquaro[3#], Lucia Carlucci[1], Lorena Zentilin[2], Ilaria Secco[2], Hashim Ali[2], Luca Braga[2], Nikoloz Gorgodze[1], Fabio Bernini[1], Silvia Burchielli[3], Chiara Collesi[2,4], Lorenzo Zandonà[4], Gianfranco Sinagra[4], Marcello Piacenti[1], Serena Zacchigna[4,5], Rossana Bussani[4], Fabio A. Recchia[1,6*], Mauro Giacca[2,4*]

[1] *Institute of Life Sciences, Scuola Superiore Sant'Anna, Pisa, Italy, Fondazione Toscana Gabriele Monasterio, 56127 Pisa, Italy.*

[2] *Molecular Medicine Laboratory, International Centre for Genetic Engineering and Biotechnology (ICGEB), 34149 Trieste, Italy*

[3] *Fondazione Toscana Gabriele Monasterio, 56127 Pisa, Italy*

[4] *Department of Medical, Surgical and Health Sciences, University of Trieste, 34127 Trieste, Italy*

[5] *Cardiovascular Biology Laboratory, International Centre for Genetic Engineering and Biotechnology (ICGEB), 34149 Trieste, Italy*

[6] *Cardiovascular Research Center, Lewis Katz School of Medicine at Temple University, Philadelphia 19140, USA*

[#]Contributed equally to the work as first authors
[*]Both authors contributed as senior authors

Co-corresponding authors:

Mauro Giacca, MD PhD
ICGEB
Padriciano, 99
34149 Trieste, Italy
tel.: +39 040 375 7324
e-mail: giacca@icgeb.org

Fabio A. Recchia, MD PhD
Institute of Life Sciences
Scuola Superiore Sant'Anna
56100 Pisa, Italy
tel.: +39 050 883266
e-mail: fabio.recchia@santannapisa.it

Stimulating cardiac regeneration after myocardial infarction is a long sought but hitherto unachieved clinical goal. An appealing alternative to the transplantation of exogenous cells is to awaken the endogenous proliferative potential of cardiomyocytes, similar to what occurs spontaneously in amphibians and fish after cardiac damage. Here we show that an adeno-associated viral vector expressing human microRNA-199a is capable of stimulating cardiac regeneration in infarcted pigs. One month after myocardial infarction and vector delivery, the treated animals showed marked improvements in both global and regional contractility, increased muscle mass and reduced scar size. These functional and morphological findings correlated with microRNA-199a-induced cardiomyocyte de-differentiation and proliferation. At longer follow-up, however, persistent and uncontrolled expression of the microRNA transgene resulted in sudden arrhythmic death of several of the treated pigs around week 7 from treatment. These events correlated with myocardial infiltration of proliferating cells showing a poorly differentiated myoblastic phenotype. Our results show that achieving cardiac regeneration through the stimulation of endogenous cardiomyocyte proliferation is attainable in large mammals, but also that the delivery of the pro-proliferative stimulus needs to be tightly controlled.

Prompt coronary catheterization and revascularization have dramatically improved the outcome of myocardial infarction (MI), but also have resulted a growing number of survived patients with permanent structural damage to the heart, which frequently leads to heart failure. This condition represents a largely unmet clinical need and one of the leading causes of mortality and morbidity in all regions of the world [1].

Post-infarction heart failure is largely due to the incapacity of the adult heart to generate a significant number of new cardiomyocytes (CMs) after birth. Carbon dating of CM DNA indicated that the renewal capacity of the heart is less than 50% over a 70-year lifetime [2]. Consistently, imaging mass spectrometry showed that CM renewal is in the order of approximately 1% every year [3]. The attempt to replace the lost myocardial tissue through the implantation of stem cells from various sources (bone marrow and the heart itself in particular [4,5]) has led to disappointing results so far, since these cells can exert a therapeutic effect in a paracrine fashion, yet they are not themselves endowed with a confirmed regenerative capacity [6]. As an alternative, new CMs can be generated ex vivo from embryonic stem (ES) or induced-pluripotent stem (iPS) cells and subsequently implanted in the damaged heart either by direct delivery [7] or in the context of engineered cardiac tissue [8,9]. However, ex vivo generation of a very large number of CMs to be implanted remains challenging and these cells are rather immature, often resulting in the generation of arrhythmias [10].

The neonatal mammalian heart immediately after birth [11] and the heart from urodeles and fish during their entire life [12,13] are instead capable of spontaneous regeneration. In all these cases, new CM formation occurs through the partial de-differentiation of already existing CMs, followed by their proliferation [11,14,15]. In adult mammals, CM proliferation is also marginally increased after cardiac damage [3], but this remains far below clinically significant levels. Thus, empowering the endogenous capacity of CM proliferation after damage in adult mammalian organisms represents a potentially exciting, new strategy to induce cardiac regeneration.

One powerful mean to modify the biological program of a cell, including its proliferation, is through interference with its microRNA (miRNA) network. Both miRNA mimics and inhibitors can be delivered to CMs to manipulate their properties, including their capacity to either enter or exit the cell cycle (reviewed in ref. 16). In particular, previous high throughput screening work from our laboratory has shown that a few human miRNAs are capable of stimulating neonatal rat and mouse CM entry into the cell cycle. Cardiac delivery of viral vectors expressing two of the most potent of those miRNAs (miR-590 and miR-199a) were effective at stimulating cardiac regeneration after MI in mice [17].

Translation of small animal work to the clinic is a formidable challenge due to key differences between rodents and large mammals, relative to cardiac anatomy, physiology and molecular regulation of CM function. Here we describe the delivery of a serotype 6-adeno-associated virus (AAV6) vector expressing

the phylogenetically conserved miR-199a after MI in pig hearts, revealing unprecedented regenerative properties of this miRNA within the first month of treatment, but also subsequent adverse effects associated with its uncontrolled, permanent expression.

RESULTS

AAV6 efficiently transduces porcine myocardium

We compared the transduction efficiency of AAV6, AAV8 and AAV9 carrying the reporter gene EGFP in porcine myocardium after intramyocardial injection in the left ventricular (LV) wall (n=3; $1x10^{12}$ v.g. per injection per animal). These three AAV serotypes have been reported to transduce post-mitotic tissues at high efficiency (reviewed in ref. [18]). By quantifying viral DNA and EGFP mRNA one month after injection, we found that AAV6 had the highest transduction efficiency in our settings (**Suppl. Fig. 1**) and was thus selected as the vector for all subsequent studies. AAV6 vectors were generated containing the hsa-miR-199a-1 pri-miRNA gene under the control of the CMV promoter; the sequences of both miR-199a-3p and miR-199a-5p, produced from this pri-miRNA, are completely conserved in rats, mice, pigs and humans (**Suppl. Fig. 2**).

Persistent and functional expression of miR-199a after AAV6-mediated delivery in infarcted pigs

Myocardial infarction (MI) was induced in 25 pigs by occlusion of the left anterior coronary artery followed by reperfusion. Animals were randomly divided into 2 groups receiving intramyocardial injection of either $2x10^{13}$ empty AAV6 (AAV6-Control) or the same dose of AAV6-hsa-miR-199a (AAV6-miR-199a; **Fig. 1a**) in the LV wall. An additional group of sham operated animals served as control. In a group of animals that had received AAV6-miR-199a we systematically assessed the levels of transgene expression through the LV. First, the heart was sectioned in four 1-cm thick slices, starting from the apex towards the base; then, each slice was divided into 2-8 regions (**Suppl. Fig. 3**). Expression of miR-199a peaked in the injected sectors. Cumulatively, the amounts of hsa-miR-199a-3p in the injected areas were increased by 18 and 26 folds at 12 and 28 days, respectively, compared to endogenous levels ($P<0.01$ in both cases; **Fig. 1b**). We also wanted to visualise exogenous miR-199a-3p expression in the transduced hearts at the single cell level. For this purpose, we developed an in situ hybridisation technique using a locked nucleic acid (LNA) probe against this miRNA. A scrambled probe and a probe for nuclear U6, which is expressed in all cell types, served as controls. Expression of miR-199a-3p was robust in cardiomyocytes (**Fig. 1c**) and specific for the injected areas throughout the left ventricle (**Suppl. Fig. 4**).

Experiments performed in mice indicated that miR-199a-3p directly targets the 3'UTRs of at least three critical genes controlling CM proliferation; two of these are factors in the Hippo pathway (the upstream inhibitory TAO kinase1 [TAOK1 [19,20]] and the phospho-YAP E3 ubiquitin-ligase β-transducing repeat containing protein [β-TrCP] [21]) while the third one is the actin cytoskeleton regulatory protein Cofilin2 [22] (data not shown). Instead, miR-199a-5p, which is also expressed at comparable levels upon cardiac miR-199a transgene expression (**Suppl. Fig. 5e**), is known to target the HIF-1α transcription factor [23]. Target sites for these miRNAs are conserved in swine (**Suppl. Fig. 5a-d**). We actually found that the expression of all four genes was downregulated in AAV6-miR-199a-treated animals (**Suppl. Fig. 5f**). Together, this information is consistent with the capacity of AAV vectors to induce robust, persistent and functional exogenous transgene expression in the myocardium [18].

The levels of viral DNA in myocardium of the injected animals were >18 times higher than in liver and >40 times higher than in other organs (spleen, kidney and lung; **Suppl. Fig. 5g**). The amount of hsa-miR-199a-3p RNA was not elevated in any analysed organ, except for the heart (**Suppl. Fig. 5h**). No overt signs of pathology, including hyper-proliferation (assessed by Ki67 staining) were observed (data not

shown). Thus, AAV6 transduction and transgene expression remain relatively localized at the sites of intramyocardial injection.

AAV6-miR-199a reduces post-infarct scar size

Morphological and functional assessment was performed using cardiac magnetic resonance imaging (cMRI). Twelve infarcted pigs from the AAV-Control and 13 from the AAV-miR-199a groups were scanned 4 weeks post-MI. A subset of animals, randomly selected from both groups (n=7 and n=8 respectively), were also scanned at 2 days post-MI to quantify myocardial oedema based on enhanced T2-weighted signals (**Fig. 1d**) to compare the extent of the initial ischemic/reperfused myocardial region [24]. No significant difference in oedema size was detected between the AAV6-Control and AAV6-miR-199a (**Fig. 1e**), indicating that the area affected by ischemia/reperfusion was similar in the two groups.

The mass of damaged myocardium was identified and quantified by cMRI based on gadolinium delayed contrast-enhanced images (late gadolinium enhancement, LGE). At 2 days post-MI, the gadolinium-retaining region, defined as either infarct mass or size, was not significantly different between the AAV6-Control and AAV6-miR-199a groups, in agreement with the measurements of oedema extension (**Fig. 1f**). At 4 weeks post-MI, both scar mass and size in the AAV-Control group were not significantly different compared to the gadolinium retaining-myocardium quantified at day 2; in contrast, the AAV6-miR-199a group displayed an over 50% reduction in scar mass and size compared to AAV6-Control (**Figs. 1f**). Paired analysis in the 8 animals that were analysed at both 2 and 28 days indicated that AAV6-miR-199a treatment resulted in decrease of scar mass by 46.2±7.7% and scar/LV mass by 48.9±5.4% from day 2 to day 28, while all those parameters did not change significantly in the AAV6-Control animals (**Suppl. Figs. 6a-c**).

Representative LGE-cMRI images of 5 cross-sectional planes (a-e, **Fig. 1g**) of hearts from 2 AAV-Control and 2 AAV6-miR-199a pigs at days 2 and 28 after MI are shown in **Fig. 1h**. A marked reduction in scar size (identified by red counterstain) at day 28 compared to the damaged area at day 2 is appreciable in the animals that received AAV6-miR-199a (the original images without counterstain are in **Suppl. Fig. 7**). For two other representative animals, gross anatomy of cardiac slices with corresponding LGE-MR images in AAV6-Control and AAV6-miR-199a at day 28 after MI are shown in **Figs. 1i** and **1j**, respectively.

The infarct region included a core fibrotic area and a surrounding grey zone, composed of a mixture of viable myocardium and fibrotic areas (**Fig. 1k**). At 28 days post-MI, the core was smaller in the AAV6-miR-199a group compared to AAV6-Control, while the gray zone was not significantly different between the two groups, consistent with a lower core/gray zone ratio in the group that benefited from miR-199a expression ($P<0.05$; **Fig. 1l**). Both the reduced scar size and the increased proportion of mixed tissue compared to fully fibrous tissue were suggestive of a process of regeneration driven by miR-199a expression in the infarct border zone.

Altogether, these findings are concordant in showing that the intramyocardial injection of AAV6-miR-199a after MI progressively reduces infarct size during the first month of treatment and increases the muscular component within the infarcted area.

Recovery of global and regional cardiac function in miR-199a-treated animals

Multiple functional parameters were analysed by cMRI in animals treated with either AAV6-Control or AAV6-miR-199a and in sham operated animals. The LV ejection fraction was recovered at 28 days in the animals injected with AAV6-miR-199a, while it remained more than 20 points below sham values in AAV6-Control ($P<0.05$ between AAV6-Control and AAV6-miR-199a; **Fig. 2a**). There was no significant difference in heart rate among the three groups (**Suppl. Fig. 8**). Similarly, LV stroke volume at day 28 in animals treated with AAV6-miR-199a returned to levels similar to those of sham animals, also indicative of improved global contractile function (**Fig. 2b**). This was mainly due to the partial recovery of the LV

end-systolic volume in the AAV6-miR-199a group, while LV end-diastolic volume was not significantly changed (**Figs. 2c** and **2d**). cMRI short axis movies of two infarcted animals, treated with either AAV6-Control or AAV6-miR-199a, are shown at 4 weeks after treatment in **Suppl. Movie 1**.

In addition to global cardiac function, cMRI was also used to assess regional/segmental contractility, as AAVs were injected selectively along the MI border zone and thus global contractility indexes might underestimate their effect [25]. Regional function was assessed by MRI-tagging **(Fig. 2e**) to measure radial strain (E_{RR}) and circumferential strain (E_{CC}). These two indexes were evaluated along short-axis LV slices (basal, middle, and apical) divided into 8 equal circumferential segments, starting from the line of attachment of the right ventricle to the LV, which served as the reference point (**Fig. 2f**). The values for E_{RR} and E_{CC}, obtained for each segment, were plotted to generate curves (**Fig. 2g** and **2h** respectively); the area under the curve (AUC [25,26]) was then calculated to integrate all the values along the LV circumference (scheme in **Fig. 2i**). This segmental analysis revealed a significant recovery of both E_{RR} and E_{CC} in the AAV6-miR-199a group compared to sham at 28 days after MI (**Figs. 2j** and **2k**). Systolic LV wall thickening was also assessed, with no need for tagging, using the same approach, yielding similar results (**Figs. 2l** and **2m**). Finally, we semi-quantitatively assessed myocardial perfusion using the 'first-pass' method, based on the injection of a bolus of gadolinium, immediately followed by image acquisition [27]. No significant differences were detected between the two groups in any LV region and at any time point (data not shown).

Taken together, these findings indicate that the morphological improvements in hearts expressing miR-199a were paralleled by significant recovery of global and regional cardiac contractile function.

AAV6-miR-199a induces cardiomyocyte proliferation

We sought changes at cellular and molecular level that could explain the reduced infarct size and improved cardiac function in the AAV6-miR-199a-treated pigs. Our previous work had shown that the delivery of the same miRNA-expressing vector, using the AAV9 capsid, induced CM proliferation and cardiac regeneration in mice [17]. To test whether a similar effect was also induced in porcine hearts, we injected either AAV6-Control or AAV6-miR-199a in an additional set of pigs (n=5 per group) subjected to ischemia and reperfusion as above. These animals received 10 daily intramuscular injections of BrdU every day from day 2 to day 12 after MI and were then sacrificed (**Figs. 3a**). In the infarct border zone of the pigs that received AAV6-miR-199a, we observed the presence of CMs positive for the proliferation marker Ki67 (8.1% of CM in the injected area compared to 1.9% in control animals; $P<0.05$; **Fig. 3b** and **Suppl. Fig. 9a** as detected by immunohistochemistry and immunofluorescence respectively). This was consistent with an increase in CMs with BrdU-positive nuclei (an S-phase marker; 8.5% vs. 2.2%; $P<0.05$ (**Fig. 3c**), staining for phosphorylated histone H3 (pH3, a marker of transition through G2/M; 0.65% vs. 0.19%; $P<0.05$ (**Fig. 3d** and **Suppl. Fig. 9b**) and, occasionally in the miR-199a group only, Aurora B kinase localization in mid-bodies, marking cells undergoing cytokinesis (**Fig. 3e**).

Pigs CMs are heavily multinucleated [28]. We detected up to 8 nuclei per CM in our pigs, but this distribution was not significantly different in control and treated animals. BrdU-positive nuclei always belonged to mono- or bi-nucleated cells (**Figs. 3f** and **3g** for quantification and representative images respectively and **Suppl. Fig. 10** for criteria used for quantification). Thus, at least at 12 days after treatment, BrdU incorporation most likely reflected cell division and/or bi-nucleation rather than multinucleation. This is also consistent with the detection of phospho-H3-positive, mitotic nuclei within mono- or bi-nucleated CMs in hearts injected with AAV6-miR-199a, as shown in **Suppl. Fig. 9b**. There was no significant difference in the cross-sectional area between BrdU-positive and BrdU-negative CMs (**Figs. 3h** and **3i**).

Another set of animals underwent to the same MI protocol and treatment with either AAV6-Control or AAV6-miR-199a (n=5 per group) but was injected with BrdU from day 20 to day 30 to assess late proliferation (**Suppl. Fig. 11a**). At this time point, analysis of Ki67 and pH3 revealed that proliferation was almost extinguished (**Suppl. Fig. 11b** and **11c**, respectively). Only a few CMs in the AAV-miR-199a

group still resulted positive for BrdU (8.8% vs. 3.1%; $P<0.05$), most likely indicative of still ongoing duplications over the 10 days prior to sacrifice (**Suppl. Fig. 11d**). Thus, replication was quenched at one month after treatment (**Suppl. Fig. 11e** and **11f**).

Collectively these data show that the expression of miR-199a delivered via AAV6 markedly boosts endogenous CM proliferation during the first weeks after MI.

Re-expression of developmental markers parallels increased cardiomyocyte proliferation

Concordant with the cMRI data, we observed a significant reduction of the fibrotic area in the infarcted region at 28 days after MI and vector injection (representative images from four different animals per group and related quantifications are provided in **Figs. 4a** and **4b** respectively). In the infarct border zone, where AAV6-miR-199a had been injected and had stimulated CM proliferation, we observed of a vast number of cells with CM morphology expressing GATA4, a transcription factor essential for cardiac development [29] and known to be re-expressed during zebrafish heart regeneration [15]. GATA4 normally localizes in the nucleus where it promotes transcription of cardiac specific genes, but can also be found in the cytoplasm during embryonic development [30].. In the animals treated with AAV6-miR-199a, a relatively large number of CMs showed GATA4 cytoplasmic localization at both 12 and 30 days after MI and vector injection (2.5% of cytoplasmic GATA4 CMs vs. 0.5% in treated and control animals at day 12, respectively; $P<0.05$; **Figs. 4c**). The staining of various cardiac areas showed the presence of GATA4-positive CMs in the infarct border, but not in the remote zones of the same hearts (**Suppl. Fig. 12**).

We then attempted to identify the molecular correlates of the effects induced by AAV6-miR-199a. First, we wondered whether the markedly increased proliferation at 12 days together with the presence of CMs showing signs of de-differentiation, might affect the structural integrity of the cardiac electrical syncytium. In animals treated with AAV6-miR-199a, we found that nuclear division, as detected by phospho-H3 staining, occurred in the context of cells that were still connected to one another via intact connexin-43 (CX43) desmosomes at intercalated discs, suggestive of proper electrical integration of the newly formed cells in the cardiac tissue (**Fig. 4d**). Consistent with preservation of cardiac function, the ratio between transcripts for adult α- and foetal β-myosin heavy chains was also preserved by AAV6-miR-199a in the infarct border, but not in the remote zone of the treated animals at both 12 and 30 days after treatment (**Fig. 4e**). A trend towards preservation from global maladaptive hypertrophy by miR-199a was also observed at 30 days both macroscopically post-mortem (one representative heart per group is shown in **Suppl. Fig. 13a)** and at histological examination, upon staining heart sections with wheat germ agglutinin to quantify CM sectional area (**Suppl. Figs. 13b** and **13c**). There were no significant differences in the levels of pathological muscle and vascular markers in the miR-199a-treated animals compared to infarcted controls, including desmin (which is essential for maintaining structural and functional integrity of myocytes [31] and was expressed at normally high levels), myogenin (which coordinates skeletal myogenesis and repair [32] and was not expressed), endothelin-B receptor (which selectively stained arterioles smooth muscle cells) and Wilms' tumour protein 1 (Wt1, which was expressed at low levels in the vascular endothelium, but not in myocytes) (**Suppl. Fig. 13d)**. Both atrial natriuretic peptide (ANP) and brain natriuretic peptide (BNP) were increased at 12 days and 30 days after MI, while this response was significantly blunted in the animals treated with AAV6-miR-199a ((**Suppl. Fig. 13e** and **13f** respectively). No differences were detected in the levels of DAB2, SMARCA5 and DESTRIN, which other studies had indicated to be altered along with CM de-differentiation [33-35] (**Suppl. Fig. 14**). Finally, we analysed vessel density by staining endothelial cells with fluorescinated lectin and arterioles using an anti-α-SMA antibody. No significant difference between the two MI groups was detected in capillary density at either 12 or 30 days (**Fig. 4f**).

Collectively, these findings are concordant in showing that increased cardiac regeneration in pigs receiving miR-199a was paralleled by the expression of the developmental marker GATA4 in the absence of overt signs of cardiac maladaptive hypertrophy or vascular pathology.

Sudden death and pathological findings in the longer term after treatment with AAV6-miR-199a despite morphological and functional recovery

A subset of infarcted animals treated with AAV6-Control (n=9) and AAV6-miR-199a (n=10) was followed for a longer time. Three of the AAV6-miR-199a pigs were analysed at 8 weeks by cMRI and continued to show persistent beneficial effects on cardiac morphology and function, with progressive reduction of cardiac scar (LGE-cMRI images showing 4 cross-sectional planes at 1, 4 and 8 weeks in this animal and in a representative AAV6-Control animal shown in **Fig. 5a**; original images without red counterstain in **Suppl. Fig. 15a**). cMRI images over time of a second pig along with gross cardiac morphology after euthanasia at 2 months are shown in **Suppl. Figs. 15b** and **15c** respectively.

Despite this progressive morpho-functional improvement until seemingly complete restoration, 7 out of 10 pigs in the of AAV6-miR-199a group died from sudden death during weeks 7-8, in the absence of preceding clinical signs. Their mortality was significantly higher compared to AAV6-Control, in which only one death was recorded after the first 8 weeks (**Fig. 5b**). In two of the pigs treated with AAV6-miR-199a and subcutaneously implanted with miniaturized recorders (Reveal, Medtronic) it was possible to record the final phases of ECG preceding sudden death, showing tachyarrhythmia events that had evolved into ventricular fibrillation (**Suppl. Fig. 16**).

Fatal arrhythmias might have occurred as a consequence of a direct or indirect effect of miR-199a on ion channels controlling cardiac electric activity. However, analysis of the expression levels of 14 different ion channels or associated protein genes involved in various types of arrhythmogenic conditions did not reveal significant differences between miR-199a-treated and control animals. Analysis of Serca2A levels, which were increased in the treated animals consistent with preservation of cardiac function, served a control in these measurements (**Suppl. Fig. 17**).

Careful examination of haematoxylin-eosin-stained tissue sections of pigs injected with AAV6-miR-199a revealed the occasional presence of small clusters of cells infiltrating the myocardium (shown for one of the pigs that survived after 8 weeks in **Fig. 5c**). These cells were negative for the leukocyte common antigen CD45 and for CD34 (excluding their immune, hematopoietic or endothelial origin) and were highly proliferating, as inferred from virtually complete positivity for Ki67. These cells also scored negative for markers of muscle differentiation, including desmin (identifying myogenic cells of cardiac, smooth and striated muscle), sarcomeric α-actinin (which labels Z lines in the cardiac and skeletal muscle sarcomere) and HHF35 (a monoclonal antibody recognizing muscle-specific α- and γ-actin); cells were also negative for Wt1 (marking several malignancies). The infiltrating cells, however, were positive for a few antigens known to be expressed during early myogenic development, including two main myogenic transcription factors (GATA4, which is critical for proper mammalian cardiac development), and myogenin (the reactivation of which characterizes rhabdomyosarcoma cells) as well as the calmodulin-binding protein caldesmon (which regulates smooth muscle contraction and is expressed at high levels in leiomyoma and leiomyosarcoma) and the endothelin-B receptor, normally expressed in smooth muscle cells. Thus, these cells express markers of early muscular differentiation. Additional clusters of these cells infiltrating the myocardium of the miR-199a-treated animals are shown in **Suppl. Fig. 18**.

We wondered whether these highly proliferating, GATA4+ and myogenin+ cells expressed miR-199a as a continuous trigger for proliferation. In situ hybridization experiments, however, indicated that the clustered cells were negative for miR-199a expression while being surrounded by CMs expressing this miRNA (**Fig. 5d**).

No additional pathological cell expansion nor evident tumours were found during necropsy in any of the treated animals.

DISCUSSION

The use of miRNAs as genetic tools to stimulate cardiac proliferation is appealing, as it leverages the capacity of these molecules to regulate the expression of multiple genes simultaneously. In contrast to individual gene knock-down or knock-out, this pleiotropic effect appears advantageous when the goal is to awake a complex process such a CM de-differentiation and proliferation. Here, cMRI, histological and molecular analysis of infarcted pig hearts were all concordant in showing that the intra-myocardial injection of AAV6-miR-199a reduced infarct size, diminished cardiac fibrosis and improved contractile function. While the extension of myocardial damage was similar between control- and miR-199a-treated animals at 2 days after MI, cMRI at one month showed significant improvement of ejection fraction and other functional parameters in the miR-199a group, indicating a recovery of global cardiac performance. At the same time point, regional contractility in the injected areas was also significantly improved. The progressive reduction of the infarct fibrous core hinted at a regenerative process activated by miR-199a overexpression and healing the damaged myocardium. This mechanism was supported by histological analyses showing increased CM proliferation in the infarct border at 12 days after vector injection. In accordance with improved contractility and favourable tissue remodelling, ANP and BNP mRNA levels were decreased while the myosin isoforms Myh6/ Myh7 ratio and the levels of Serca2a were increased in the miR-199a-expressing myocardium.

Could myocardial tissue recovery and improved cardiac function be ascribed to an additional effect of AAV6-miR-199a on CM survival? At least two considerations argue against this possibility. First, our previous work has tested whether miR-199a-3p also protected cells from death either ex vivo or after MI, and failed to identify such property [17,36]. Similarly, no difference in the number of TUNEL-positive CMs was found in the present study in hearts excised 12 days after infarction and AAV vector administration (not shown). Second, the increase in cardiac mass observed by cMRI in the AAV6-miR-199a animals correlated with the presence of relatively numerous BrdU-positive and Ki67-positive cells in the infarct border zone, at the sites of vector injection. These cells not only entered the cell cycle (Ki67 positivity) and synthesized new DNA (BrdU incorporation), but also progressed through G2/M phases (positivity for phosphorylated H3) and, more occasionally, showed localization of the Aurora B kinase in midbodies, a marker of cell division. Of interest, re-entry of CMs into the cell cycle was limited to mono- or bi-nucleated cells.

When analysing CM proliferation in the miR-199a-treated animals, we found that the proliferative activity of these cells was relatively high at 12 days after MI and vector administration, while it was significantly quenched at one month. This result is tends to indicate that the stimulus exerted by miR-199a is essential, albeit not sufficient, to drive CM proliferation. Effective proliferation would also require a proper permissive environment, likely generated by the inflammatory conditions immediately after MI. This conclusion appears consistent with our observation that the injection of AAV vectors expressing miR-199a in non infarcted pig hearts exerts no apparent effect (**Suppl. Fig. 19**).

A peculiar finding in the AAV6-miR-199a-treated pigs was the presence, in the infarct border zone, of a remarkable number of GATA4-positive cells, suggestive of CM de-differentiation. During embryonic heart development in both mice and fish, GATA4 regulates the final steps of CM differentiation, driving the expression of numerous cardiac genes, including α-myosin heavy chain and cardiac troponin C [29,37]. After cardiac damage in zebrafish, de novo expression of GATA4 stimulates the de-differentiation of CMs, inducing a phenotype permissive for their division and characterized by looser and de-structured sarcomeres [15].

To evaluate the long-term effect of constitutive miR-199a expression, a number of animals were monitored for more than a month. Despite progressively smaller scar size and improved cardiac function observed by cMRI, 7 out of 10 animals treated with AAV6-miR-199a died of sudden cardiac death between day 45 and 55. Three of these animals carried implanted ECG mini-recorders and, in two of them we were able to record an episode of ventricular fibrillation that preceded their death. The origin of these lethal arrhythmias possibly causing sudden death is unknown at the moment. Of note, these terminal

events occurred at similar time points, i.e. at approximately 1.5 months after treatment. This is consistent with the possibility that the pro-proliferative effect of miR-199a-3p might have generated areas of poorly-differentiated cells that, by progressively growing in size, eventually formed fatal re-entry electric circuits. This explanation appears more plausible than a direct arrhythmogenic effects of miR-199a itself due to the targeting of genes involved in cardiac excitation-contraction coupling or conduction. If this were the case, we would have expected earlier arrhythmias. In addition, none of the screened ion channels known to be involved in the generation of arrhythmias were downregulated in the AAV6-miR-199a-treated animals.

In this context, it is important to mention that, in pig hearts, AAV-mediated delivery of the miR-199a precursor DNA also leads to the generation of miR-199a-5p,. Therefore, we cannot exclude that adverse electrical events were the consequence of the long-term, unwanted expression of miR-199a-5p, which is known to induce hypertrophy[38,39] and other deleterious effects [40,41] in rodent hearts.

In some of the animals that died of sudden death, as well as in the two that survived for 60 days, histological analysis revealed the presence of small clusters of highly proliferating (Ki67-positive) cells infiltrating the cardiac tissue. These cells expressed markers of undifferentiated cells of muscle origin, among which myogenin, caldesmon and GATA4. Thus, they appear to possess the phenotypic identity of myoblasts at the early stages of differentiation. Of interest, proliferation of these cells was unlikely driven by the continuous expression of miR-199a-3p, since they were not labelled by an anti-miR-199a LNA probe, although they were located in areas of homogenous CM transduction and miRNA expression. We conclude that either the cells had lost the AAV6 vectors due to their replication (AAVs do not integrate into the host cell genome [18]) or they arise as a consequence of an altered microenvironment caused by cytokines and growth factors produced by CMs primarily transduced by AAV9-miR-199a. Single-cell genomics characterization of these cells will help clarifying this issue. Whether these cell clusters constituted a potential arrhythmogenic substrate remains to be determined. Of note, we did not find a clear correlation between the presence of these clusters and sudden death, as the heart with the highest number and extension of them was from a pig that survived for 8 weeks after MI and AAV9-miR-199a delivery and displayed remarkable regeneration (shown in **Fig. 5a**).

In summary, our study shows that AAV6-miR-199a delivery improves cardiac function and reduces scar size and fibrosis in infarcted juvenile pigs by stimulating CM de-differentiation and cell cycle re-entry. Conversely, its long-term expression causes sudden cardiac death. Thus, it appears that a therapy based on the constitutive expression of miR-199a through AAV-mediated gene delivery is not feasible for human translation. Despite this caveat, the concept that cardiac regeneration after MI might be achieved through the stimulation of the endogenous capacity of CM to proliferate, rather than the transplantation of exogenous cells, is definitely supported by our observations. As for any other drug, microRNA therapy needs to be properly weighted in dose and time of administration, a requisite that is beyond the properties of virus-mediate gene delivery. Our past work, however, has indicated that, in the mouse, synthetic miRNA mimics can be administered to the heart in complex with cationic lipids and that a single administration of miR-199a-3p exerts an effect lasting at least 12 days, which is sufficient to elicit a regenerative response [36]. Synthetic miR-199a-3p administration can be precisely dosed and is devoid of the untoward effects exerted by the miRNA passenger strand. Whether the administration of this synthetic mimic will also be effective in triggering cardiac regeneration in infarcted large animals in the absence of undesired long-term effects is thus an exciting possibility, which is worth pursuing with an eventual translational perspective.

ACKNOWLEDGMENTS

This work was supported by the European Research Council (ERC) [Advanced Grants 250124 and 787971] to MG; the Leducq Foundation Transatlantic Network of Excellence [grant 14CVD04]; the Fondazione CRTrieste [Project CTC], Trieste, Italy and the Italian Ministry of Health [grant RF-2011-

02348164 “CardioRigen”]. GP, IS and HA are supported by an ICGEB Arturo Falaschi pre-doctoral Fellowship. The authors are grateful to Marina Dapas and Michela Zotti from the ICGEB AAV Unit for AAV vector production.

AUTHORS CONTRIBUTIONS

MG and FAR designed the experiments and supervised the project. KG, LC, NG, FB and SB performed the in vivo pig experimentation. GA supervised cardiac assessment by cMRI. GP, IS, HA, LB and CC performed molecular and immufluorescence analysis. RB and LZ performed histological and immunohistochemistry analysis. SZ provided essential advice for the experimental design. LZ supervised production of AAV vectors. MP and GS provided expert advice on electrophysiology and heart failure studies.

REFERENCES

1 Roth, G. A. *et al.* Global, Regional, and National Burden of Cardiovascular Diseases for 10 Causes, 1990 to 2015. *J Am Coll Cardiol* **70**, 1-25, (2017).

2 Bergmann, O. *et al.* Evidence for cardiomyocyte renewal in humans. *Science* **324**, 98-102, (2009).

3 Senyo, S. E. *et al.* Mammalian heart renewal by pre-existing cardiomyocytes. *Nature* **493**, 433-436, (2013).

4 Garbern, J. C. & Lee, R. T. Cardiac stem cell therapy and the promise of heart regeneration. *Cell Stem Cell* **12**, 689-698, (2013).

5 Henry, T. D., Moye, L. & Traverse, J. H. Consistently Inconsistent-Bone Marrow Mononuclear Stem Cell Therapy Following Acute Myocardial Infarction: A Decade Later. *Circ Res* **119**, 404-406, (2016).

6 Eschenhagen, T. *et al.* Cardiomyocyte Regeneration: A Consensus Statement. *Circulation* **136**, 680-686, (2017).

7 Chong, J. J. *et al.* Human embryonic-stem-cell-derived cardiomyocytes regenerate non-human primate hearts. *Nature* **510**, 273-277, (2014).

8 Tiburcy, M. *et al.* Defined Engineered Human Myocardium With Advanced Maturation for Applications in Heart Failure Modeling and Repair. *Circulation* **135**, 1832-1847, (2017).

9 Weinberger, F. *et al.* Cardiac repair in guinea pigs with human engineered heart tissue from induced pluripotent stem cells. *Sci Transl Med* **8**, 363ra148, (2016).

10 Anderson, M. E., Goldhaber, J., Houser, S. R., Puceat, M. & Sussman, M. A. Embryonic stem cell-derived cardiac myocytes are not ready for human trials. *Circ Res* **115**, 335-338, (2014).

11 Porrello, E. R. *et al.* Transient regenerative potential of the neonatal mouse heart. *Science* **331**, 1078-1080, (2011).

12 Oberpriller, J. O. & Oberpriller, J. C. Response of the adult newt ventricle to injury. *J Exp Zool* **187**, 249-253, (1974).

13 Poss, K. D., Wilson, L. G. & Keating, M. T. Heart regeneration in zebrafish. *Science* **298**, 2188-2190, (2002).

14 Jopling, C. *et al.* Zebrafish heart regeneration occurs by cardiomyocyte dedifferentiation and proliferation. *Nature* **464**, 606-609, (2010).

15 Kikuchi, K. *et al.* Primary contribution to zebrafish heart regeneration by gata4(+) cardiomyocytes. *Nature* **464**, 601-605, (2010).

16 Giacca, M. & Zacchigna, S. Harnessing the microRNA pathway for cardiac regeneration. *J Mol Cell Cardiol* **89**, 68-74, (2015).

17 Eulalio, A. *et al.* Functional screening identifies miRNAs inducing cardiac regeneration. *Nature* **492**, 376-381, (2012).

18 Zacchigna, S., Zentilin, L. & Giacca, M. Adeno-associated virus vectors as therapeutic and investigational tools in the cardiovascular system. *Circ Res* **114**, 1827-1846, (2014).

19 Plouffe, S. W. *et al.* Characterization of Hippo Pathway Components by Gene Inactivation. *Mol Cell* **64**, 993-1008, (2016).

20 Poon, C. L., Lin, J. I., Zhang, X. & Harvey, K. F. The sterile 20-like kinase Tao-1 controls tissue growth by regulating the Salvador-Warts-Hippo pathway. *Dev Cell* **21**, 896-906, (2011).

21 Zhao, B., Li, L., Tumaneng, K., Wang, C. Y. & Guan, K. L. A coordinated phosphorylation by Lats and CK1 regulates YAP stability through SCF(beta-TRCP). *Genes Dev* **24**, 72-85, (2010).

22 Xue, B. & Robinson, R. C. Guardians of the actin monomer. *Eur J Cell Biol* **92**, 316-332, (2013).

23 Rane, S. *et al.* Downregulation of miR-199a derepresses hypoxia-inducible factor-1alpha and Sirtuin 1 and recapitulates hypoxia preconditioning in cardiac myocytes. *Circ Res* **104**, 879-886, (2009).

24 Lindsey, M. L. *et al.* Guidelines for Experimental Models of Myocardial Ischemia and Infarction. *Am J Physiol Heart Circ Physiol*, (2018).

25 Simioniuc, A. *et al.* Placental stem cells pre-treated with a hyaluronan mixed ester of butyric and retinoic acid to cure infarcted pig hearts: a multimodal study. *Cardiovasc Res* **90**, 546-556, (2011).

26 Koch, K. C. *et al.* Myocardial viability assessment by endocardial electroanatomic mapping: comparison with metabolic imaging and functional recovery after coronary revascularization. *J Am Coll Cardiol* **38**, 91-98, (2001).

27 Nagel, E. *et al.* Magnetic resonance perfusion measurements for the noninvasive detection of coronary artery disease. *Circulation* **108**, 432-437, (2003).

28 Grabner, W. & Pfitzer, P. Number of nuclei in isolated myocardial cells of pigs. *Virchows Arch B Cell Pathol* **15**, 279-294, (1974).

29 Molkentin, J. D., Lin, Q., Duncan, S. A. & Olson, E. N. Requirement of the transcription factor GATA4 for heart tube formation and ventral morphogenesis. *Genes Dev* **11**, 1061-1072, (1997).

30 Chen, D. *et al.* Dual function of the UNC-45b chaperone with myosin and GATA4 in cardiac development. *J Cell Sci* **125**, 3893-3903, (2012).

31 Li, Z. *et al.* Desmin is essential for the tensile strength and integrity of myofibrils but not for myogenic commitment, differentiation, and fusion of skeletal muscle. *J Cell Biol* **139**, 129-144, (1997).

32 Zammit, P. S. Function of the myogenic regulatory factors Myf5, MyoD, Myogenin and MRF4 in skeletal muscle, satellite cells and regenerative myogenesis. *Semin Cell Dev Biol* **72**, 19-32, (2017).

33 Kubin, T. *et al.* Oncostatin M is a major mediator of cardiomyocyte dedifferentiation and remodeling. *Cell Stem Cell* **9**, 420-432, (2011).

34 Aguirre, A. *et al.* In vivo activation of a conserved microRNA program induces mammalian heart regeneration. *Cell Stem Cell* **15**, 589-604, (2014).

35 Wang, W. E. *et al.* Dedifferentiation, Proliferation, and Redifferentiation of Adult Mammalian Cardiomyocytes After Ischemic Injury. *Circulation* **136**, 834-848, (2017).

36 Lesizza, P. *et al.* Single-Dose Intracardiac Injection of Pro-Regenerative MicroRNAs Improves Cardiac Function After Myocardial Infarction. *Circ Res* **120**, 1298-1304, (2017).

37 Gupta, V. *et al.* An injury-responsive gata4 program shapes the zebrafish cardiac ventricle. *Curr Biol* **23**, 1221-1227, (2013).

38 Zhang, H. *et al.* Qiliqiangxin Attenuates Phenylephrine-Induced Cardiac Hypertrophy through Downregulation of MiR-199a-5p. *Cell Physiol Biochem* **38**, 1743-1751, (2016).

39 Song, X. W. *et al.* MicroRNAs are dynamically regulated in hypertrophic hearts, and miR-199a is essential for the maintenance of cell size in cardiomyocytes. *J Cell Physiol* **225**, 437-443, (2010).

40 el Azzouzi, H. *et al.* The hypoxia-inducible microRNA cluster miR-199a approximately 214 targets myocardial PPARdelta and impairs mitochondrial fatty acid oxidation. *Cell Metab* **18**, 341-354, (2013).

41 Li, Z. *et al.* miR-199a impairs autophagy and induces cardiac hypertrophy through mTOR activation. *Cell Death Differ* **24**, 1205-1213, (2017).

42 Ayuso, E. *et al.* Manufacturing and characterization of a recombinant adeno-associated virus type 8 reference standard material. *Hum Gene Ther* **25**, 977-987, (2014).

43 Arsic, N. *et al.* Vascular endothelial growth factor stimulates skeletal muscle regeneration in vivo. *Mol Ther* **10**, 844-854, (2004).

44 Slavin, G. S. & Saranathan, M. FIESTA-ET: high-resolution cardiac imaging using echo-planar steady-state free precession. *Magn Reson Med* **48**, 934-941, (2002).

45 Masci, P. G. *et al.* Myocardial salvage by CMR correlates with LV remodeling and early ST-segment resolution in acute myocardial infarction. *JACC Cardiovasc Imaging* **3**, 45-51, (2010).

46 Lionetti, V. *et al.* Mismatch between uniform increase in cardiac glucose uptake and regional contractile dysfunction in pacing-induced heart failure. *Am J Physiol Heart Circ Physiol* **293**, H2747-2756, (2007).

47 Bogaert, J. & Rademakers, F. E. Regional nonuniformity of normal adult human left ventricle. *Am J Physiol Heart Circ Physiol* **280**, H610-620, (2001).

48 Atkinson, D. J., Burstein, D. & Edelman, R. R. First-pass cardiac perfusion: evaluation with ultrafast MR imaging. *Radiology* **174**, 757-762, (1990).

49 Positano, V. *et al.* Myocardial perfusion by first pass contrast magnetic resonance: a robust method for quantitative regional assessment of perfusion reserve index. *Heart* **92**, 689-690, (2006).

50 Chan, R. H. *et al.* Prognostic value of quantitative contrast-enhanced cardiovascular magnetic resonance for the evaluation of sudden death risk in patients with hypertrophic cardiomyopathy. *Circulation* **130**, 484-495, (2014).

51 Schmidt, A. *et al.* Infarct tissue heterogeneity by magnetic resonance imaging identifies enhanced cardiac arrhythmia susceptibility in patients with left ventricular dysfunction. *Circulation* **115**, 2006-2014, (2007).

METHODS

Production and purification of recombinant AAV vectors. Hsa-miR-199a was amplified from human genomic DNA isolated from HeLa cells, using the QIAamp DNA mini kit (Qiagen), according to the manufacturer's instructions, as previously described [17.] The amplified sequence was cloned into the pZac2.1 vector (Gene Therapy Program, Penn Vector core, University of Pennsylvania, USA), which was used to produce recombinant AAV vectors. Recombinant AAV vectors were prepared in the AAV Vector Unit at ICGEB Trieste, as described previously [42]. In particular, AAV serotype 6 vectors were generated in HEK293T cells, by co-transfecting the plasmid vector together with the packaging plasmid pDP6 (PlasmidFactory, Germany).

Viral stocks were obtained by PEG precipitation and two subsequent $CsCl_2$ gradient centrifugations. Titration of AAV viral particles was performed by real-time PCR quantification of the number of packaged viral genomes, as described previously [43]; the viral preparations had titres between $1.3x10^{13}$ and $3.3x10^{13}$ viral genomes per ml.

Open chest surgery and myocardial infarction. Three- to four-month old male farm pigs, weighting 28-32 kg, were sedated with a cocktail of 4 mg/kg tiletamine hydrochloride and 4 mg/kg zolazepam hydrochloride injected intramuscularly, intubated and mechanically ventilated with positive pressure. Inhalatory anaesthesia was maintained by a mixture of 1-2% isoflurane dissolved in 40% air and 60% oxygen. Electrocardiogram (ECG), heart rate and arterial pressure were constantly monitored. A thoracotomy was performed in the left fourth intercostal space and then the pericardial sac was opened to expose the heart. A small group of animals (n=3) received direct intramyocardial injections of $1x10^{12}$ v.g. AAV6, AAV8 and AAV9, suspended in PBS and carrying the reporter gene eGFP, in 3 separate sites of the LV anterior wall, one vector serotype for each site, to compare their transduction efficiency.

Myocardial infarction (MI) was induced by coronary occlusion in 19 pigs anesthetized and operated as described above. Thirty min before coronary occlusion, pigs were medicated with 4.3 mg/kg of amiodarone in 500 ml of 0.9% sodium chloride to prevent arrhythmias. The left anterior descending coronary artery (LAD) was isolated from surrounding tissue distal to the first diagonal branch, encircled by a suture (**Suppl. Fig. 20a**); the two ends of the suture were threaded through a plastic tube and tightened to achieve occlusion of the vessel, confirmed by the presence of regional myocardial cyanosis, ST segment elevation in the ECG and ventricular arrhythmias, which were more pronounced within the first 30-45 min. The LAD occlusion was removed after 90 min to start the reperfusion phase.

After 10 min of reperfusion, the survived animals were randomized in 2 groups receiving: $2x10^{13}$ empty AAV6 (AAV6-control; n=12) or $2x10^{13}$ AAV6-hsa-miR-199a-3p (AAV6-miR-199a; n=13). The viral particles were suspended in 2 ml of PBS and delivered by 20 direct intramyocardial injections equally spaced along the border zone (100 µl per injection). This latter was visually identified as the margin of the ischemic myocardium (pale compared to the normally perfused myocardium; **Suppl. Fig. 20b**). Some of the injection sites were tagged with coloured epicardial stitches to detect and sample the corresponding myocardial tissue post-mortem for histological analysis. An additional group of sham-operated animals was operated in the same manner, but LAD was not ligated (sham; n=6). In this experimental setting, the delivery of the vector at the time of MI allows avoiding a second surgery a few days/hours after MI, which would importantly increase animal mortality.

At the end of the study, animals were anaesthetized and sacrificed by injection of 10% KCl to stop the heart at diastole. The excised hearts were sectioned through four horizontal planes and each section was then subdivided into sub-sections for further histological and molecular analysis as shown in **Suppl. Figs. 3** and **4**). Briefly, each heart was sectioned in four 1-cm thick slices, starting from the apex towards the base. Then, each slice was divided into 2-8 regions (indicated by letters in the Figure). In all

quantifications, we have considered at least 8 sectors of the four heart sections. Sectors H, T and C corresponded to the infarct border zone, where the vectors were administered, while sector L was considered representative of the remote zone, since it was on the same plane but on the opposite position (posterior) relative to sector T. Each region was then divided into 2 pieces (for RNA analysis and histology, respectively) by a transversal cut in order to keep both the endocardial and pericardial borders visible in each piece. For all quantifications, the same regions were chosen in animals injected with either control or miR-199a vectors.

LV assessment with cMRI. Cardiac magnetic resonance imaging was performed at 2 days and 4 weeks after MI. Animals were sedated with a cocktail of 4 mg/kg tiletamine hydrochloride and 4 mg/kg zolazepam hydrochloride injected intramuscularly and light anesthesia was maintained by continuous intravenous infusion of propofol (30-40 mcg/kg/min) at spontaneous respiration. Pigs were placed in a right lateral position with the heart at the isocenter on MRI unit. ECG was monitored continuously.

cMRI images were acquired with a clinical 1.5 T scanner (Signa Excite HD; GE Medical Systems, Waukesha, WI, USA), using a non-breath-hold ECG gated, multi-NEX steady-state free precession pulse sequence (fast imaging employing steady-state acquisition) [44]. The heart was scanned along two long axis views (vertical and horizontal) and with a set of short axis views covering the entire LV from atrioventricular valve plane to the apex. The following parameters were used: field of view 30 cm, slice thickness 8 mm, no gap between each slice, repetition time 3.7 msec, echo time 1.6 msec, views for segment 2, flip angle 45°, bandwidth 125 Hz, 30 phases, matrix 224 x 224, reconstruction matrix 256 x 256, NEX 3, free breathing. Myocardial oedema at 2 days post-MI was identified using T2-weighted short-tau inversion-recovery fast spin echo pulse sequence. The sequence parameters were field of view 30 cm; slice thickness: 8 mm, TR: 2 R-R intervals, TE: 100 ms, TI: 150 ms, matrix: 256 × 256 [45]. The main functional characteristics of pigs treated with either AAV6-Control or AAV6-miR-199a as detected by cMRI at different time points are summarised in **Suppl. Table I**.

Tagging-cMRI images were acquired with an electrocardiography-gated, segmented K-space, fast gradient recalled echo pulse sequence with spatial modulation of magnetization to generate a grid tag pattern. Nonselective radiofrequency pulses separated by spatial modulation of magnetization-encoding gradients allowed tag separation of 10 mm. Three sets of short-axis at basal, middle and apical level views were acquired with a grid of tags line with 45° angulation. The number of views per phase was optimized based on heart rate. The following parameters were used: field of view 30 cm, slice thickness 8 mm, no gap between each slice, repetition time 8 msec, echo time 4.3 msec, flip angle 12°, bandwidth 31 Hz, 30 phases, matrix 192 x 192, reconstruction matrix 256 x 256, NEX 3.

Myocardial perfusion imaging was performed using a first pass technique with the injection of the contrast agent Gd-DTPA (0.2 mmol/kg iv) and an ECG-gated interleaved saturation recovery gradient echo planar imaging pulse sequence. Three short axis images (basal, middle and apical) were acquired for each beat for 60 consecutive beats.

To identify the scar and quantify the extension of post-infarction fibrosis, delayed enhanced images were acquired in two-dimensional T1 weighted segmented inversion recovery-prepared gradient echo-sequence 5-10 min after administration Gd-DTPA (0.2 mmol/kg iv) in short- and long-axis views correspondent to those of cine-cMR. The following parameters were used: field of view 30 mm, slice thickness 8 mm, no gap between each slice, repetition time 4.6 msec, echo time 1.3, flip angle 20°, matrix 224 x 192, reconstruction matrix 256 x 256, number of excitation 3.

Reveal (Medtronic) implantation involved a 2-cm cutaneous incision behind the left scapula. The device was inserted inside a subfascial pocket with the electrodes facing outward. Device data collection was activated by the programmer with R-wave sensing threshold of 0.12 mV to automatically detect arrhythmias. The parameters for episode detection were set as follows: FVT (interval 300 ms, duration 12/16 beats), VT (interval 360 ms, duration 16 beats), brady (interval 2000 ms, duration 4 beats), asystole (duration 3 sec) and AF (all episodes).

cMRI Image analysis. Randomized images were analysed in a blinded manner under the supervision of a III-level EACVI (European Association of Cardiovascular Imaging) cardiac MRI accredited cardiologist, using commercially available research software package (Mass 6, Leyden, The Netherlands). In the acute phase of MI, the region corresponding to infarct-related oedema was defined based on a signal intensity 2 times higher than the mean SI of normal myocardium on T2 weighted images. The oedema border was defined by manually tracking the hyperintense region on T2-weighted, short-axis images and the oedema size expressed as a percentage of total LV mass [45].

Global LV functional parameters (end-diastolic volume and end-systolic volume, ejection fraction) and left ventricular regional wall thickening (LVWT) were measured as previously described [25,46]. LV endocardial and epicardial borders were manually traced on all short-axis cine images at the end-diastolic and end-systolic frames to determine the end-diastolic and end-systolic volumes, respectively, as well as ejection fraction and cardiac mass. The same software was used to calculate LVWT. Briefly, the middle slice (area of interest), orthogonal to LV long axis, at 30% of its length starting from the apex, was divided into 8 equal circumferential segments (**Fig. 2f**). The inferoseptal segment at the connection of the right ventricle with the left ventricle was defined as a reference point for the ventricular segmentation. Eight segments were plotted to generate the curve and subsequently calculate the area under the same curve (AUC) [26]; **Fig 2i**).

The analysis of tagged cardiac images was performed using a custom software based on the method by Bogaert et al. [47]. The two-dimensional maximal circumferential (E_{CC}) and radial strain (E_{RR}) were evaluated along short-axis LV slices, basal, middle, and apical, divided into 8 equal circumferential segments, starting from the reference point of the ventricular segmentation (**Fig. 2f**). The values for E_{CC} and E_{RR}, obtained for each segment, were plotted to generate curves, as in the case of LVWT (**Fig. 2g** and **2h**, respectively) and, subsequently, the AUC was calculated to integrate all the values along the LV circumference (scheme in Fig. **2i**).

Myocardial regional perfusion was assessed with the first-pass technique [48]. The first pass segmental time-signal intensity curves, expressed as arbitrary unit/time, relative to different LV regions were generated using the Mass 6 software [49]. Perfusion was evaluated semiquantitatively with signal intensity/time curves by calculating the relative upslope corresponding to the maximal signal intensity change during the wash-in phase for 18 segments obtained by sectioning the LV along three parallel short-axis planes, each divided in 6 segments.

To detect post-infarction fibrosis and determine its size, the LV short-axis stack of LGE images was first assessed visually for the presence of LGE. The quantification of LGE was then performed on all LGE-positive studies by manually adjusting a gray-scale threshold to define areas of visually identified LGE. These areas were then summed to generate a total volume of LGE and expressed as a proportion of total LV myocardium (%LGE; [50]). The infarct areas were also analysed using the full width half maximum method [51] to differentiate the dense infarct core from the heterogeneous gray zone ad previously described [25]. |The infarct core was defined as an area with SI > 50% of maximal SI of enhanced myocardium. The gray zone of the infarct periphery was defined as the myocardium with SI > peak of remote myocardium but <50% of maximal SI of the high SI myocardium. Finally, infarction core and the gray zone were quantified as a percentage of the total myocardium and as a percentage of the total infarct size.

DNA and RNA isolation and quantification. Total DNA was isolated using the DNeasy Blood & Tissue Kit (Qiagen) following the manufacturer's instruction and used as a template to detect and quantify vector DNA by real-time PCR. Primers and TaqMan® probe (Applied Biosystems, Foster City, CA, USA), recognising the CMV promoter driving miR-199a expression, were as described [17]. The pig housekeeping 18S rRNA gene was used as a normalizer (Thermofisher Scientific).

Total RNA, including the small RNA fraction, was isolated from pig tissue fragments using the miRNeasy Mini Kit (Qiagen) according to the manufacturer's instruction. DNAse treatment was performed during RNA isolation according to the manufacturer's protocol. For gene expression analysis, total RNA was quantified by Nanodrop and reverse transcribed using hexameric random primers followed by qRT-PCR using Taqman assays (Applied Biosystems) for Myh6, Myh7, ANP and BNP, according to the manufacturer's instruction. The housekeeping GAPDH was used for normalization.

For miR-199a-3p quantification, total RNA was reverse transcribed using miRCURY LNA PCR synthesis kit (Exiqon) and qRT-PCR was performed with pre-designed miRCURY LNA PCR primer sets (Exiqon) and miRCURY LNA SYBR Green master mix according to the manufacturer's instructions. MicroRNA expression was normalized on the expression levels of 5S rRNA.

Histological and immunofluorescence analyses. The hearts were briefly washed in PBS, weighted, sectioned as described above and fixed in 10% formalin at room temperature, embedded in paraffin and further processed for histology or immunofluorescence. Haematoxylin–eosin and Masson's trichrome staining (Bioptica) were performed according to standard procedure and analysed for morphology; extent of fibrosis was measured on 4x magnification images using ImageJ.

For immunostaining, pig heart sections were deparaffinized in xylene and rehydrated. Antigen retrieval was performed by boiling samples in sodium citrate solution (0.1 M, pH 6.0) for 20 min. Sections were let cool down and permeabilised for 20 min in 1% Triton X-100 in PBS, followed by blocking in 1% BSA (Roche). Sections were then stained overnight at 4°C with the following primary antibodies diluted in blocking solution, recognizing the following antigens: sarcomeric α-actinin (Abcam), Ki67 (Monosan), histone H3 phosphorylated at serine 10 (Millipore), Aurora B kinase (Sigma), GATA4 (Abcam), desmin (Roche), myogenin (Cell Marque), endothelin receptor B (Abcam), Wt1 (Cell Marque), CD34 (Roche), CD45 (Roche). Sections were washed with PBS and incubated for 2 h with the respective secondary antibodies conjugated with Alexa Fluor-488, -555 or -647 (Life Technologies). Nuclei were stained with Hoechst 33342 (Life Technologies). Alternatively, after endogenous peroxidase inhibition with 3% H_2O_2, sections were incubated with appropriate biotin-conjugate secondary antibody (Abcam) in TBS-BSA 1% for 1 h at room temperature. Following signal amplification with Avidin–Biotin-Complex-HRP (VECTASTAIN), DAB solution (VECTOR) was applied for 3 to 10 min. Hematoxylin (Bioptica) was further use to stain nuclei.

For BrdU incorporation analysis, after section permeabilisation, DNA denaturation was obtained by incubating 10 min in 1M HCl on ice and 20 min in 2M HCl at 37°C. Sections were further incubated with 0.1 M sodium-borate buffer pH 8.4 for 12 min at room temperature, washed three times with PBS and then blocked for 1 h in 10% horse serum PBS. Tissue sections were stained overnight at 4°C with anti-α-actinin antibody (Abcam) in 5% horse serum PBS and in anti-BrdU (Abcam). Washes and secondary antibody incubation were performed as described above.

To measure CM cross sectional area, lectin Wheat Germ Agglutinin (WGA; Vector Labs) was diluted 1:100 in PBS and added with the secondary antibody to sample sections and incubated as described above. Capillary density was determined after staining histological sections with lectin Wheat Germ Agglutinin together with anti-α-SMA antibody (Vector Labs) diluted in PBS.

In all quantifications of immunofluorescence and immunohistochemistry images, we considered, for each animal, at least 8 sectors belonging to all four heart sections shown in **Suppl. Fig. 3**. For each region considered, histological analysis was performed by acquiring 7 high-resolution images at 20X

magnification, which were quantified by blinded researchers.

In situ hybridization. MicroRNA in situ hybridization (ISH) was performed using locked nucleic acid (LNA) probes for miR-199a-3p and U6 snRNA, as well as an oligonucleotides with the same nucleotide content as the anti-miR-199a probe but in a scrambled sequence. Experiments were performed using a MicroRNA ISH kit for Formalin-fixed paraffin-embedded (FFPE) tissues (Qiagen) according to the manufacturer's protocol. Briefly, FFPE heart tissue slides were deparaffinised in xylene, treated with proteinase-K (15 µg/ml) for 10 min at 37°C and incubated with hsa-miR-199-3p (20 nM), scramble (20 nM) and U6 probes (2 nM) for one hour at 57°C in a hybridizer. After washing with SSC buffer, miRNA expression was detected using an anti-DIG alkaline phosphatase (AP) antibody (1:800) (Roche Diagnostics) supplemented with goat serum (Jackson Immunoresearch) and NBT-BCIP substrate (Roche Diagnostics).

Statistical analysis. Data are presented as mean ± standard error of the mean (SEM). Statistical analysis was performed by employing commercially available software (GraphPad Prism). Differences among groups were compared by one- and two-way ANOVA followed by the Bonferroni post-hoc test. For survival analysis, a Kaplan-Meier survival curve was generated and log-rank statistics test was rendered. The AUC was obtained using the trapezoidal rule and statistical comparisons performed by one- and two-way ANOVA. For all the statistical analyses, significance was accepted at $P<0.05$.

FIGURE LEGENDS

Figure 1. **miR-199a treatment reduces infarct size. a**, Schematic representation of the experimental protocol. After ischemia/reperfusion and AAV6 intramyocardial injection, pigs underwent cardiac MRI at day 2 and at day 28. **b**, Graph representing miR-199a-3p quantification 12 and 28 days after infarction and vector delivery. Data are represented as fold over endogenous levels (AAV6-Control) and expressed as mean±SEM; the number of animals per group and time point is indicated. ***P*<0.01 vs. AAV6-Control at the same time point; ##*P*<0.01 vs. sham. **c**, In situ hybridization of miR-199a-3p, scrambled oligonucleotide and U6 LNA probes in pig heart sections at day 12 after treatment. Scale bar: 100 µm. **d**, Examples of T2-weighted cMRI images showing cardiac oedema (a), with corresponding late gadolinium enhancement (LGE) cMRI images (b) at day 2 post-MI. Dark myocardium is viable, infarcted area is highlighted in red for better visualization. **e**, Oedema (%LV) at two days after MI. Data are mean±SEM; the number of animals per group is indicated. ns: not significant. **f**, LGE mass (g) and size (%LV), at days 2 and 28 post-MI. Data are mean±SEM; the number of animals per group and time point is indicated. ns: not significant; **P*<0.05 vs. AAV6-Control at the same time point; #*P*<0.05 vs. AAV6-miR-199a at day 2 post MI. **g**, Schematic representation of cMRI slices, from apex to base (a to e). **h**, LGE-cMRI images (from apex to base, a to e) of four representative pig hearts, two receiving AAV6-Control and other two AAV6-miR-199a at 2 and 28 days after MI. The infarct area is counterstained in red; the corresponding original images without counterstaining are shown in **Suppl. Fig. 7 i**, **j**, Gross anatomy of cardiac slices with corresponding LGE-cMRI images in representative AAV6-Control and AAV6-miR-199a treated pig hearts, at 28 days post-MI. **k**, Identification of infarct scar and gray zone by LGE-cMRI. **l**, Infarct gray zone, infarct core and their ratio 28 days post-MI measured by LGE-cMRI. Data are mean±SEM; the number of animals per group and time point is indicated. ns: not significant; **P*<0.05 vs. AAV6-Control at the same time point.

Figure 2. **miR-199a delivery improves global and regional cardiac function. a**-**d**, LV ejection fraction (EF, %), stroke volume (ml), LV end-systolic volume (ml) and LV end-diastolic volume (ml), respectively, measured by cMRI in non-infarcted controls and infarcted animals at days 2 and 28 post-MI and either AAV6-Control or AAV6-miR-199a injection. Data are mean±SEM; the number of animals per group and time point is indicated. ns: not significant; **P*<0.05 vs. AAV6-Control at the same time point; #*P*<0.05 vs. sham; $*P*<0.05 vs. day 2. **e**, Example of cardiac short axis image with the tagging grid in diastole and systole. **f**, Subdivision of the LV short axis in 8 circumferential segments (left) and their correspondence with the infarct core, border zone and the remote zone (right). The syringe indicates the infarct border injected with AAVs. IS, inferoseptal; S, septal, AS, anteroseptal; A, anterior; AL, anterolateral; L, lateral; IL, inferolateral; I, inferior. **g, h**, Eight-segment curves corresponding to LV radial (LVErr) (g) and circumferential (LVEcc) (h) strain at 28 days after MI. **P*<0.05 vs. AAV6-Control; #*P*<0.05 vs. sham. **i**, Schematic example of calculation of the area under curve (AUC) in arbitrary units. **j, k,** AUC for Err (j) and Ecc (k). Data are mean±SEM; the number of animals per group is indicated. **P*<0.05 vs. AAV6-Control; #*P*<0.05 vs. sham. **l**, Eight-segment curves corresponding to LV end-systolic wall thickening (LVWT) at 28 days after MI. **P*<0.05 vs. AAV6-Control; #*P*<0.05 vs. sham. **m**, AUC for LVWT. Data are mean±SEM; the number of animals per group is indicated. **P*<0.05 vs. AAV6-Control; #*P*<0.05 vs. sham.

Figure 3. **AAV6-miR-199a injection induces cardiomyocyte proliferation in vivo**. **a**, Schematic representation of the protocol. Animals underwent ischemia-reperfusion and concomitant AAV6 injection. At day 2 after surgery, they were injected daily with BrdU until sacrifice at day 12. **b**, Representative Ki67 immunohistochemistry images of the infarct border zone (BZ) in AAV6-Control- and AAV6-miR-199a-treated pigs 12 days after surgery, and relative quantification. The bottom panels are high magnification images of the indicated portions of the upper images. Data are mean±SEM; the

number of animals per group is indicated. *P<0.05. Scale bar: 100 µm. **c**, **d,** Representative images of BrdU (c) and phospho-histone H3 (d) immunostaining in the infarct border zone of AAV6-Control- and AAV6-miR-199a-treated animals, 12 days post MI, with relative quantifications. The bottom panels are high magnification images of the indicated portion of the upper image. Data are mean±SEM; the number of animals per group is indicated. *P<0.05. Scale bar: 100 µm. **e**, Aurora B immunofluorescence images showing localization in midbodies (arrow) in AAV6-miR-199a treated animals, 12 days post MI. Scale bar: 20 µm. **f**, Distribution of the number of total and BrdU+ nuclei per CM in AAV6-Control- and AAV6-miR-199a-treated pigs 12 days after surgery. Data are mean±SEM of four pigs with at least 5 sections per pig. **g**, Representative images of multinucleated CMs with BrdU+ nuclei. WGA: wheat germ agglutinin to stain CM sarcolemma. Scale bar: 100 µm. **h**, Cross-sectional area measurements of $BrdU^+$ and $BrdU^-$ cardiomyocytes in AAV6-Control- and AAV6-miR-199a-treated pigs 12 days after surgery. Data are mean±SEM from the analysis of 4 pigs. **i**, Representative images of BrdU+ and BrdU- CM. Scale bar: 50 µm. The right panels are high magnification images of the indicated portions of the left images.

Figure 4. **Morphological and molecular characterization of AAV6-miR-199a effect in pig hearts. a**, **b**, Azan-Mallory trichrome staining representative images of transverse heart sections of four AAV6-Control and four AAV6-miR-199a injected pig hearts one month after surgery (a), with relative quantification of the area of fibrosis (b). Data are mean±SEM; the number of animals per group is indicated. *P<0.05. BZ: border zone. **c**, Representative immunohistochemistry images of GATA4-positive cells in AAV6-Control- and AAV6-miR-199a-injected pigs, 12 and 30 days after treatment along with quantification of cells showing GATA4 cytoplasmic localization. The bottom panels are high magnification images of the indicated portions of the upper images. Data are mean±SEM; the number of animals per group is indicated. Quantification is from at least 7 high-resolution images acquired from at least 8 different regions of each heart. *P<0.05. Scale bar: 100 µm. **d**, Connexin-43 (CX43, red) and phospho-histone H3 (pH3, blue-green) immunofluorescence representative images of AAV6-miR-199a-treated pig heart sections, 12 days after infarction. Scale bar: 100 µm. **e**, Real-time PCR quantification of the ratio between α- and β-myosin heavy chain mRNA in sham, AAV6-Control- and AAV6-miR-199a-injected pig hearts, at 12 and 30 days after surgery in the H (border zone) and L (remote zone) cardiac sectors (cf. **Suppl. Fig. 4**). Data are mean±SEM; the number of animals per group and time point is indicated. ns: not significant; *P<0.05 vs. AAV6-Control at the same time point. **f**, Representative sections of pig hearts treated with AAV6-Control and AAV6-miR-199a at day 30 after infarction and vector injection stained with FITC-lectin to visualize vessels and with an anti-α-SMA antibody to detect smooth muscle cells, along with quantification of lectin-positive vessels. Data are mean±SEM; the number of animals per group is indicated. *P<0.05. Scale bar: 100 µm.

Figure 5. **Long-term expression of miR-199a induces progressive cardiac regeneration but causes sudden death**. **a,** LGE-cMRI representative images, from apex to base, of AAV6-Control- and AAV6-miR-199a treated pig hearts at 2 days, 4 weeks and 8 weeks after MI. The infarct area is counterstained in red; the corresponding original images without counterstaining are shown in **Suppl. Fig. 15a**. **b**, Kaplan Meier curve showing mortality after MI and vector administration. The number of animals per group is indicated. **c**, Hematoxylin-eosin staining or immunostaining for the indicated antigens of the same cell cluster in consecutives tissue sections from an infarcted heart injected with AAV6-miR-199a at 8 weeks after treatment. Scale bar: 100 µm. **d**, In situ hybridization of miR-199a-3p, scrambled and U6 LNA probes in pig heart sections with infiltrating cell cluster. Scale bar: 100 µm.

SUPPLEMENTARY FIGURE LEGENDS

Supplementary Figure 1. **Adeno-associated virus serotype 6 (AAV6) is the most effective serotype for porcine heart transduction. a**, **b**, Graphs representing viral genomes and EGFP mRNA levels, respectively, one month after direct intramyocardial injection of 10^{12} v.g. particles of AAV6, AAV8 and AAV9 carrying the EGFP transgene. Data are mean±SEM; the number of animals per group is indicated.

Supplementary Figure 2. **MicroRNA-199a sequence and conservation among species a**, Nucleotide sequence of the miR-199a-1 precursor. Mature miR-199a-5p and miR-199a-3p sequences are in green and their seed sequences are in blue and red respectively. **b**, **c**, Mature miR-199a-5p and miR-199a-3p sequences, respectively, in human, mouse, rat and pig. The microRNA seed sequences are in blue for miR-199a-5p and in red for miR-199a-3p.

Supplementary Figure 3. **Systematic assessment of miR-199a-3p expression after AAV6-mediated transduction. a**, Schematic representation of pig heart sectioning for histological and molecular studies. After arrest in diastole, the heart was excised and the pericardial sac removed. AAV injection sites, which were marked with coloured epicardial sutures during surgery, were further traced with a green water-proof paint. Four 1-cm thick transversal slices were cut starting from the base to the apex (1 to 4 in the Figure). Each slice was subsequently divided into 2-8 regions, each one labeled with a capital letter, and then into additional sub-regions (letters plus numbers) for targeted molecular and histological analyses. Sectors H, T and C corresponded to the infarct border zone (BZ), where the vectors were administered, while sector L was considered representative of the remote zone. **b**, Injection and infarct border segments for each slice were divided into smaller fragments (dashed lines) to accurately assess the levels of expression of the transgene at 12 days after transduction. The syringe indicates the injection sites. For each slice and segment, the graphs on the right side show real-time PCR quantifications of the mature miR-199a-3p expressed as fold over endogenous levels (AAV6-Control; mean±SEM). One representative animal is shown out of four analysed in the same systematic manner, with comparable results.

Supplementary Figure 4. **In situ hybridization of pig heart sections for the detection of miR-199a expression after AAV6-miR-199a transduction**. **a**, Same as in Suppl. Fig. 3a. **b-e**, Each of the four transversal slices (1-4; pictures are the same as in Suppl. Fig. 3) was subdivided into the indicated sectors, which were individually tested by in situ hybridization using LNA probes detecting miR-199a-3p or U6 snRNA, or a probe with the same nucleotide composition as the one against miR-199a-3p but with a scrambled sequence (scramble). One representative animal is shown out of four analyzed in the same systematic manner with comparable results. Scale bar: 100 μm

Supplementary Figure 5. **Downregulation of miR-199a target genes in transduced heart tissue and organ distribution of the AAV6-miR-199a vector. a**-**c**, Predicted target sites of miR-199a-3p in the 3'UTR sequences of swine Cofilin2, TAOK1 and βTRC according to TargetScan Release 7.2. All these three genes are verified direct targets of this miRNA in rodents; the corresponding 3'UTR target sites for Cofilin2 and TAOK1 are conserved in swine; for βTRC, two alternative target sites are in swine are shown. Other miR-199a-3p target genes originally identified in mice (in particular, Homer1 and Clic5 [17,36]) are not conserved in the swine genome. In the pig genome, βTRC also has an additional predicted target sequence for miR-199a-5p, which is indicated. **d**. Predicted target site of miR-199a-5p in the 3'UTR of pig HIF-1α mRNA. **e**, Real-time PCR quantification of both strands of miR-199a in AAV6-Control- and AAV6-miR-199a-injected pig hearts normalized over endogenous 5S rRNA. Data are mean±SEM. **f**, mRNA levels of predicted and annotated target genes of miR-199a in AAV6-Control- and

AAV6-miR-199a-treated pig hearts one month after MI and viral transduction. Data are mean±SEM; *P<0.05 vs. AAV6-Control. **g**, Quantification of viral genomes in the indicated organs one month after intracardiac injection of AAV6-miR199a. Data are expressed as fold over liver levels after normalization for cellular DNA content using the 18S DNA as a reference. **h**, Levels of miR-199a-3p RNA in the indicated organs one month after intracardiac injection of AAV6-miR-199a. Data are shown as fold over endogenous miRNA levels in liver in control animals after normalization for cellular 5S rRNA.

Supplementary Figure 6. **MiR-199a improves global heart function and decreases infarct mass one month after treatment**. **a**-**c**, Graphs showing changes in infarct mass (%, a), infarct mass over left ventricle mass (%, b) and ejection fraction (%, c) between 2 and 28 days after MI and AAV delivery, measured by cMRI. Upper panels: cumulative values for all pigs (data are mean±SEM; *P<0.05); lower panels: individual pigs.

Supplementary Figure 7. Infarct healing at one month after AAV6-miR-199a injection. The LGE-cMRI images (from apex to base, a to e) are the same as in **Fig. 1h** without red counterstain. The red arrow shows the infarcted area in the central plane c.

Supplementary Figure 8. Heart rate in sham and infarcted animals injected with AAV6-Control and AAV6-miR-199a. Data are mean±SEM; the number of animals per group and time point are indicated. There was no significant difference in heart rate among the three groups.

Supplementary Figure 9. AAV6-miR-199a induces cardiomyocyte proliferation in vivo. a, Representative images of Ki67 and α-actinin immunofluorescence staining of the infarct border (sector H) or remote (sector L) zones of AAV6-Control- and AAV6-miR-199a-treated animals, 12 days post MI. Scale bar: 100 µm. **b**, High magnification representative images of phospho-histone H3 immunostaining in the infarct border zones of four different pigs treated with AAV6-miR-199a, 12 days post MI. Scale bar: 100 µm.

Supplementary Figure 10. Extent of multinucleation in pig hearts. a, Representative images of longitudinal sections stained with wheat germ agglutinin (WGA) to assess the number of nuclei per CM in the infarct border zone of AAV6-Control- and AAV6-miR-199a-treated animals, 12 days post MI. The right panels show the estimated number of nuclei for each cardiomyocyte. Scale bar: 50 µm. **b**, Additional representative images of mono- or bi-nucleated BrdU-positive CMs in the infarct border zone of AAV6-Control- and AAV6-miR-199a-treated animals, 12 days post MI. Scale bar: 50 µm.

Supplementary Figure 11. AAV6-miR-199a-mediated cardiomyocyte proliferation is blunted 30 days after infarction. **a**, Schematic representation of the experimental procedure. Animals underwent ischemia-reperfusion and concomitant AAV6 injection. At day 20 after surgery, they were injected daily with BrdU until sacrifice at day 30. **b**, Representative Ki67 immunohistochemistry images of the infarct border zone (BZ) in AAV6-Control- and AAV6-miR-199a-treated pigs 30 days after surgery, and relative quantification. The bottom panels are high magnification images of the indicated portions of the upper images. Data are mean±SEM; the number of animals per group is indicated. ns: not significant. Scale bar: 100 µm. **c**, **d,** Representative images of phospho-histone H3 (c) and BrdU (d) immunostaining in the infarct border zone of AAV6-Control- and AAV6-miR-199a-treated animals, 30 days post MI, with relative quantifications. The bottom panels are high magnification images of the indicated portion of the upper image. Data are mean±SEM; the number of animals per group is indicated. ns: not significant;

*P<0.05. Scale bar: 100 µm. **e**, **f**, Changes in the percentages of Ki67- (e) and phospho-histone H3- (f) positive CMs at days 12 and 30 after infarction and vector administration.

Supplementary Figure 12. Cardiomyocytes expressing GATA4 with cytoplasmic localization in the infarct border zone of AAV6-miR-199a-treated pigs. Low and high magnification representative immunohistochemistry images of GATA4-positive cells in the infarct border (sector H) or remote zone (sector L) of AAV6-Control- and AAV6-miR-199a-injected pigs, 12 and 30 days after treatment. Scale bar: 100 µm.

Supplementary Figure 13. Molecular correlates of miR-199a transduction. a, Representative images of 1 cm-slices from sham, AAV6-Control- and AAV6-miR-199a-treated pig hearts sectioned from apex to base. **b, c,** Lectin immunofluorescence images (b) of sham, AAV6-Control- and AAV6-miR-199a-treated pig sections, 30 days after MI and vector administration along with quantification (c) of CM cross-sectional area (μm^2). Data are mean±SEM; the number of analyzed animals is indicated. ns: not significant. Scale bar: 50 µm. **d**, Low and high magnification representative images of infarcted hearts injected with AAV6-Control or AAV6-miR-199a after immunohistochemistry to detect desmin, myogenin, Wt1 and endothelin receptor 1. Scale bar: 100 µm**. e**, **f,** Real-time PCR quantification of the levels of ANP and BNP in sham, AAV6-Control- and AAV6-miR-199a-injected pig hearts, at 12 and 30 days after surgery. Data are mean±SEM; the number of animals per group and time point is indicated. ns: not significant; *P<0.05 vs. AAV6-Control at the same time point.

Supplementary Figure 14. AAV6-miR-199a treatment does not alter the levels of DAB2, SMARCA5 and DESTRIN mRNAs. a, Real-time PCR quantification of the levels of the indicated genes in sham, AAV6-Control- and AAV6-miR-199a-injected pig hearts, at 12 and 30 days after surgery. Data are mean±SEM; the number of animals per group and time point is indicated. ns: not significant; *P<0.05 vs. AAV6-Control at the same time point.

Supplementary Figure 15. Long-term expression of miR-199a induces progressive cardiac regeneration. a, The LGE-cMRI images (from apex to base, a to e) are the same as in **Fig. 5a** without red counterstain. The red arrow shows the infarcted area in the central plane c. **b**, cMRI images from a pig sacrificed at week 8 after MI and AAV6-miR-199a treatment. The upper panels shows serial images from apex to base at day 2, week 4 and week 8; he infarct area is counterstained in red. The bottom panels show the same images without counterstaining. The green arrow shows the pacemaker lead fixation site. **c**, Gross anatomy of cardiac slices of the pig shown in panel b at sacrifice. The syringe indicates the injected area.

Supplementary Figure 16. Recording of fatal arrhythmias in two infarcted pigs treated with AAV6-miR-199a-3p. Initiation of ventricular fibrillation (red arrows) recorded at the moment of death in two AAV6-miR-199a pigs by implanted miniaturized ECG recorders (Reveal, Medtronic, 9529). **a**, A premature ventricular ectopic beat (red arrow) with a coupling interval of 380 ms during a slowing heart rhythm induced a fast ventricular tachycardia that degenerated in ventricular fibrillation. **b**, A premature ventricular ectopic beat (red arrow) with coupling interval of 290 ms induced a fast ventricular tachycardia that quickly degenerated in ventricular fibrillation of different amplitudes resembling polymorphic ventricular tachycardia.

Supplementary Figure 17. AAV6-mediated, long-term expression of miR-199a did not affect the levels of ion channels or associated proteins involved in known arrhythmogenic conditions. In the

infarct border zone of pigs treated with AAV6-Control or AAV6-miR-199a (n=6 and n=4 respectively) at 8 weeks after transduction, the expression levels of genes known to be involved in the pathogenesis of the Long QT Syndrome (Scn5a, Kcne1, Snta1, Akap9, Ank2), Brugada syndrome (Cacna1, Cacnb2, Scn1b), Carvajal syndrome (DSP), Arrhythmogenic Right Ventricular Cardiomyopathy (DSG2, DSP), Catecholaminergic Polymorphic Ventricular Tachycardia (CASQ2, Ryr2) were assesed. Additional investigated mRNAs were those coding for Serca2A (which also served as a positive control since it is depressed during heart failure), phospholamban (Pln), Connexins 40 and 43 (CX40 and CX43 respectively). Data are mean±SEM; the number of animals per group and time point is indicated. ns: not significant; *P<0.05 vs. AAV6-Control.

Supplementary Figure 18. miR-199a induces formation of proliferating cell clusters with an early myoblast phenotype infiltrating the pig myocardium. Additional images of cell clusters infiltrating the infarcted hearts injected with AAV6-miR-199a after hematoxylin-eosin staining or immunostaining for Ki67, sarcomeric α-actinin, GATA4 and myogenin. The pig identity, treatment, time of analysis and cardiac sector from which the sample was taken (according to the scheme in **Suppl Fig. 4**) are shown for each picture. Scale bar: 100 µm. Clusters of cells were never detected in control-injected animals, however in one animal injected with AAV6-miR-199a in the absence of MI.

Supplementary Figure 19. AAV6-miR-199a does not induce cardiomyocyte proliferation in non infarcted hearts. a, Schematic representation of the experimental procedure. Animals underwent open-chest AAV6-miR-199a injection and, 12 days after surgery, they were euthanised and their hearts sectioned for molecular and histological analysis of the injected area. **b**, Real-time PCR quantification of the levels of miR-199a-3p. Data are mean±SEM; the number of animals per group and time point is indicated. **P<0.01. **c**, **d**, Representative Ki67 immunohistochemistry (c) and phospho-H3 immunofluorescence (d) images of AAV6-Control- and AAV6-miR-199a-treated pigs 12 days after injection from the injected area, and relative quantification. Data are mean±SEM; the number of animals per group is indicated. Scale bar: 100 µm.

Supplementary Figure 20. **Procedure for myocardial infarction and vector injection. a, b,** Representative picture taken during porcine surgery and vector injection. After thoracotomy, the pericardial sac was opened, LAD was exposed and occluded below its first branch for 90 minutes. Ten minutes after reperfusion, AAV6-Control or AAV6-miR-199a were injected in the infarct border zone.

SUPPLEMENTARY MOVIE

Supplementary movie 1. Representative cardiac cine MR movies of AAV6-Control (**left**) and AAV6-miR-199a (**right**) pig hearts at 28 days post-MI. The short axis view shows LV cross-sections. A pronounced negative remodelling (wall thinning and chamber dilation) and dyskinesia of the LV anterior and septal walls are evident in the heart injected with AAV6-Control, while the heart injected with AAV6-miR-199a displays a markedly preserved morphology and very mild hypokinesia, closely resembling normal heart features.

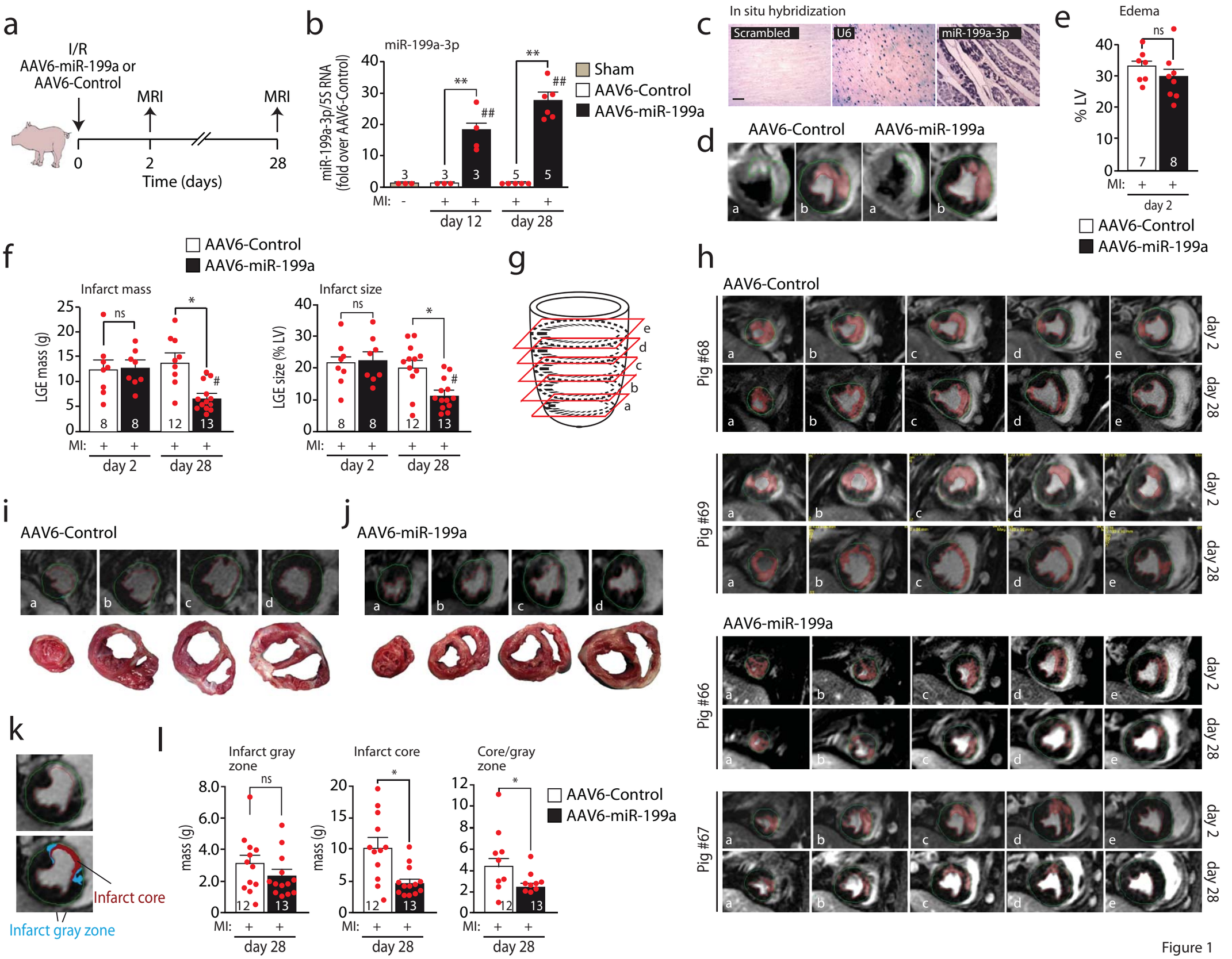
a
I/R
AAV6-miR-199a or
AAV6-Control
MRI
MRI
0
2
28
Time (days)
b
miR-199a-3p
miR-199a-3p/5S RNA
(fold over AAV6-Control)
Sham
AAV6-Control
AAV6-miR-199a
MI:
day 12
day 28
c
In situ hybridization
Scrambled
U6
miR-199a-3p
d
AAV6-Control
AAV6-miR-199a
e
Edema
% LV
MI:
day 2
AAV6-Control
AAV6-miR-199a
f
AAV6-Control
AAV6-miR-199a
Infarct mass
LGE mass (g)
Infarct size
LGE size (% LV)
MI:
day 2
day 28
g
h
AAV6-Control
Pig #68
Pig #69
AAV6-miR-199a
Pig #66
Pig #67
day 2
day 28
i
AAV6-Control
j
AAV6-miR-199a
k
Infarct core
Infarct gray zone
l
Infarct gray zone
Infarct core
Core/gray zone
mass (g)
AAV6-Control
AAV6-miR-199a
MI:
day 28

Figure 1

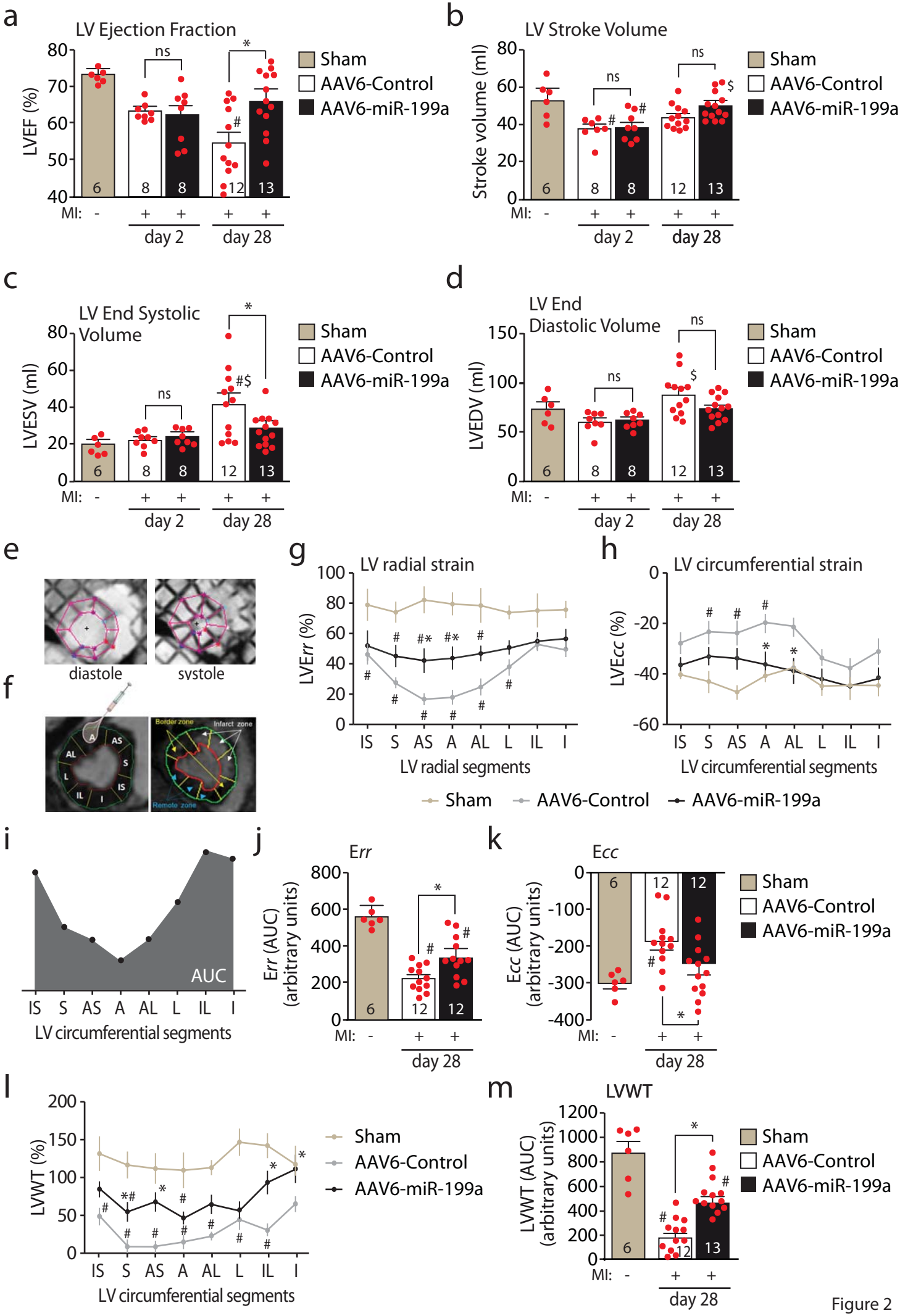
a
LV Ejection Fraction
LVEF (%)
ns
*
#
Sham
AAV6-Control
AAV6-miR-199a
MI: - + + + +
day 2
day 28
b
LV Stroke Volume
Stroke volume (ml)
ns
#
$
c
LV End Systolic Volume
LVESV (ml)
#$
d
LV End Diastolic Volume
LVEDV (ml)
e
diastole
systole
f
Border zone
Infarct zone
Remote zone
A
AS
S
IS
I
IL
L
AL
g
LV radial strain
LVErr (%)
IS S AS A AL L IL I
LV radial segments
h
LV circumferential strain
LVEcc (%)
LV circumferential segments
i
AUC
LV circumferential segments
j
Err
Err (AUC) (arbitrary units)
k
Ecc
Ecc (AUC) (arbitrary units)
l
LVWT (%)
LV circumferential segments
m
LVWT
LVWT (AUC) (arbitrary units)

Figure 2

a

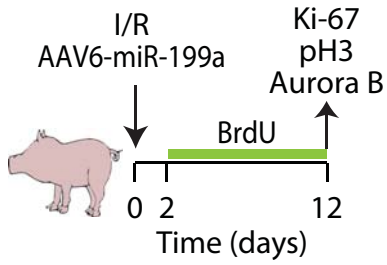

b

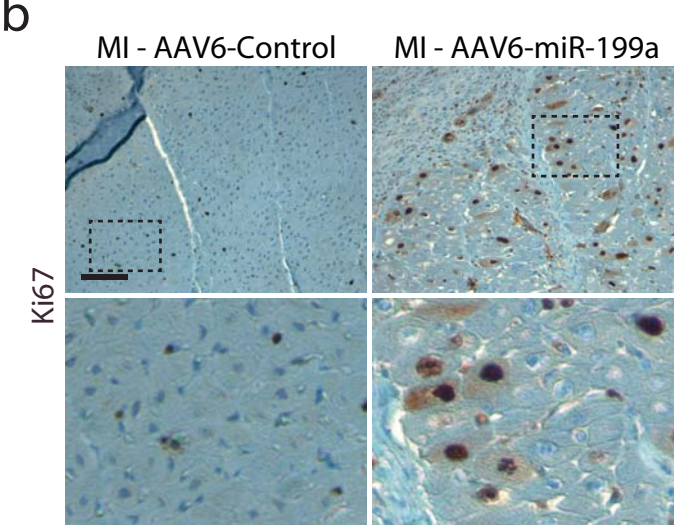

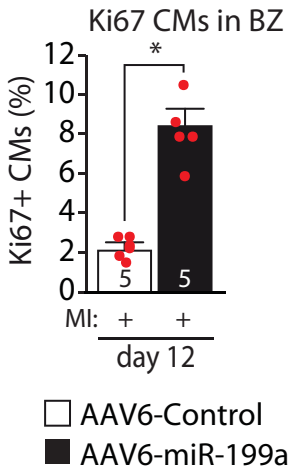

c

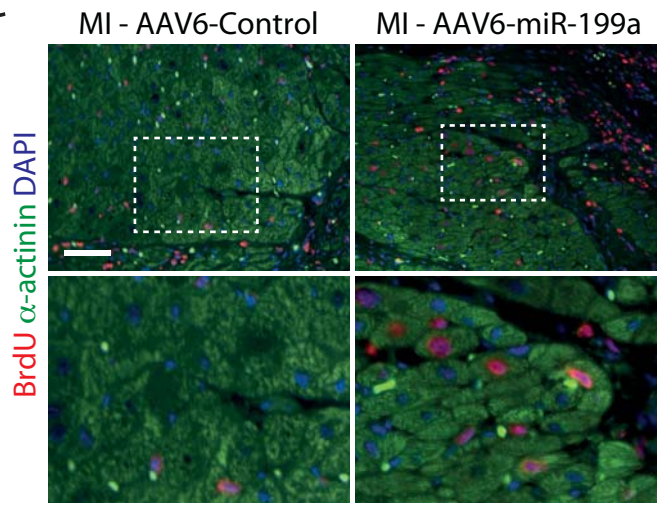

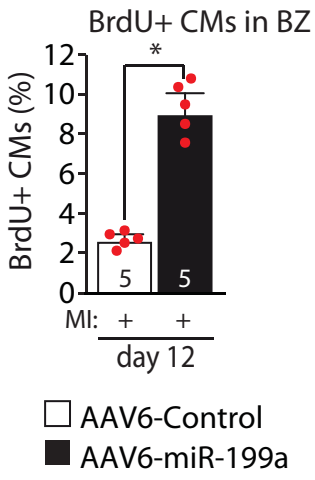

d

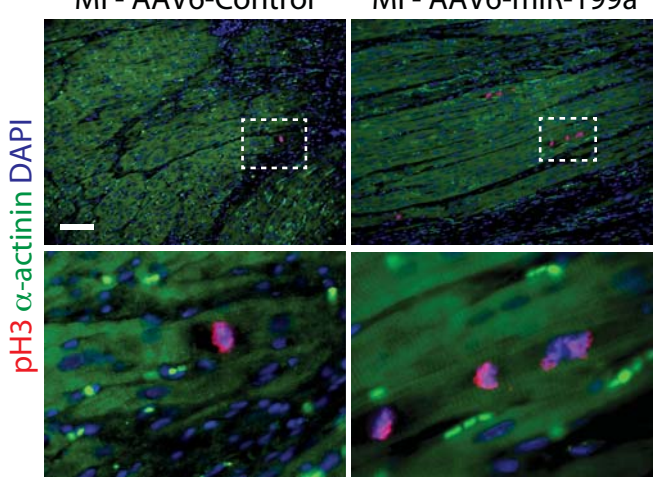

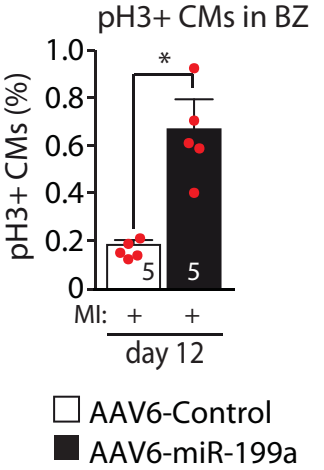

e

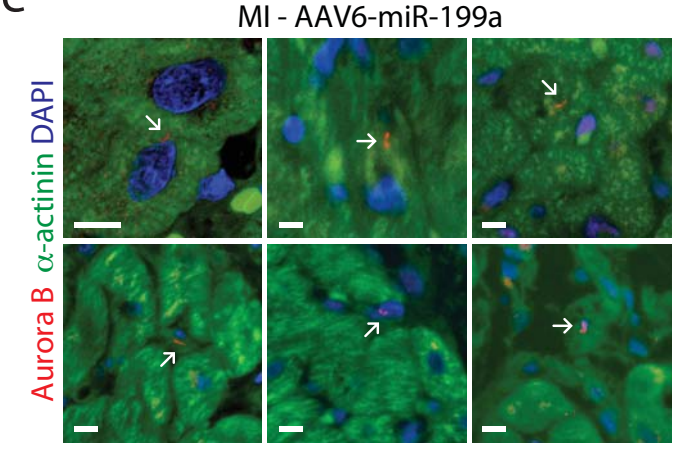

f

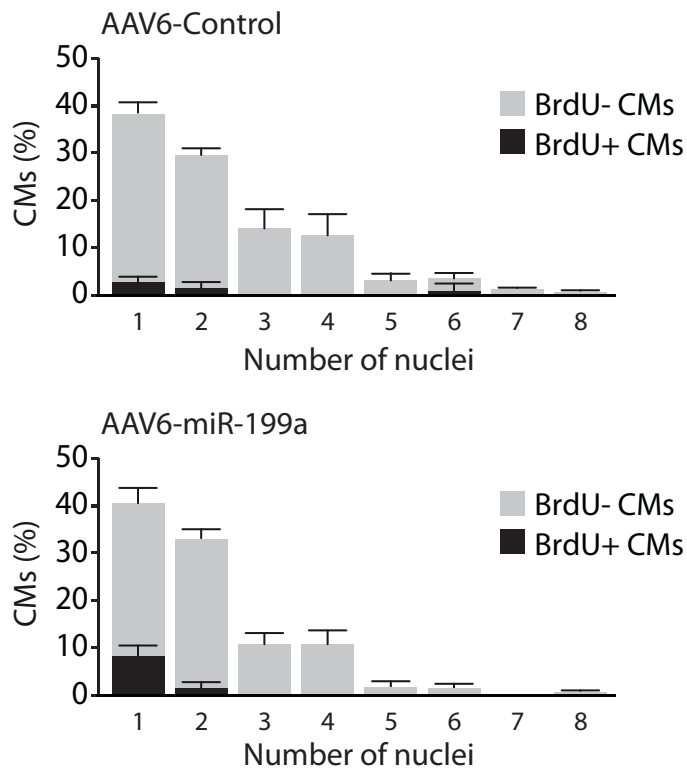

g

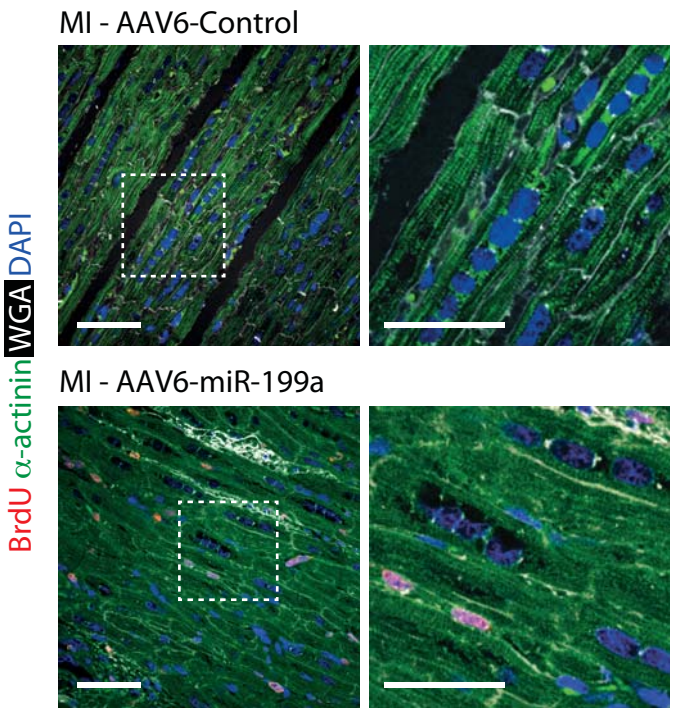

h

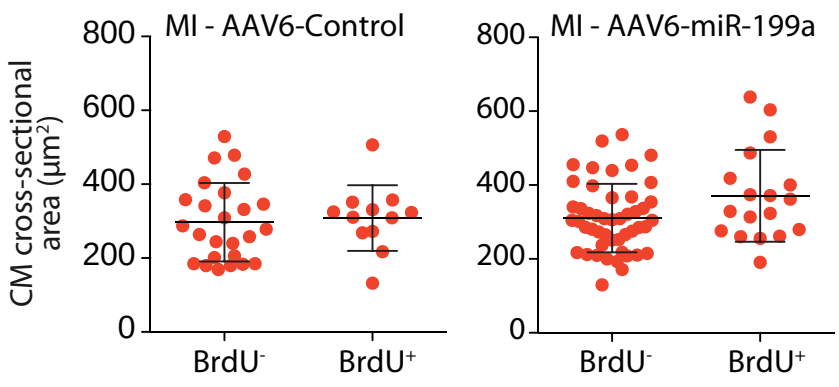

i

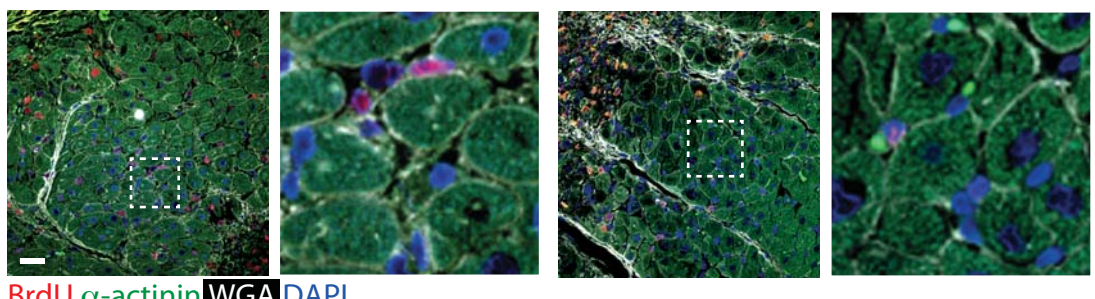

Figure 3

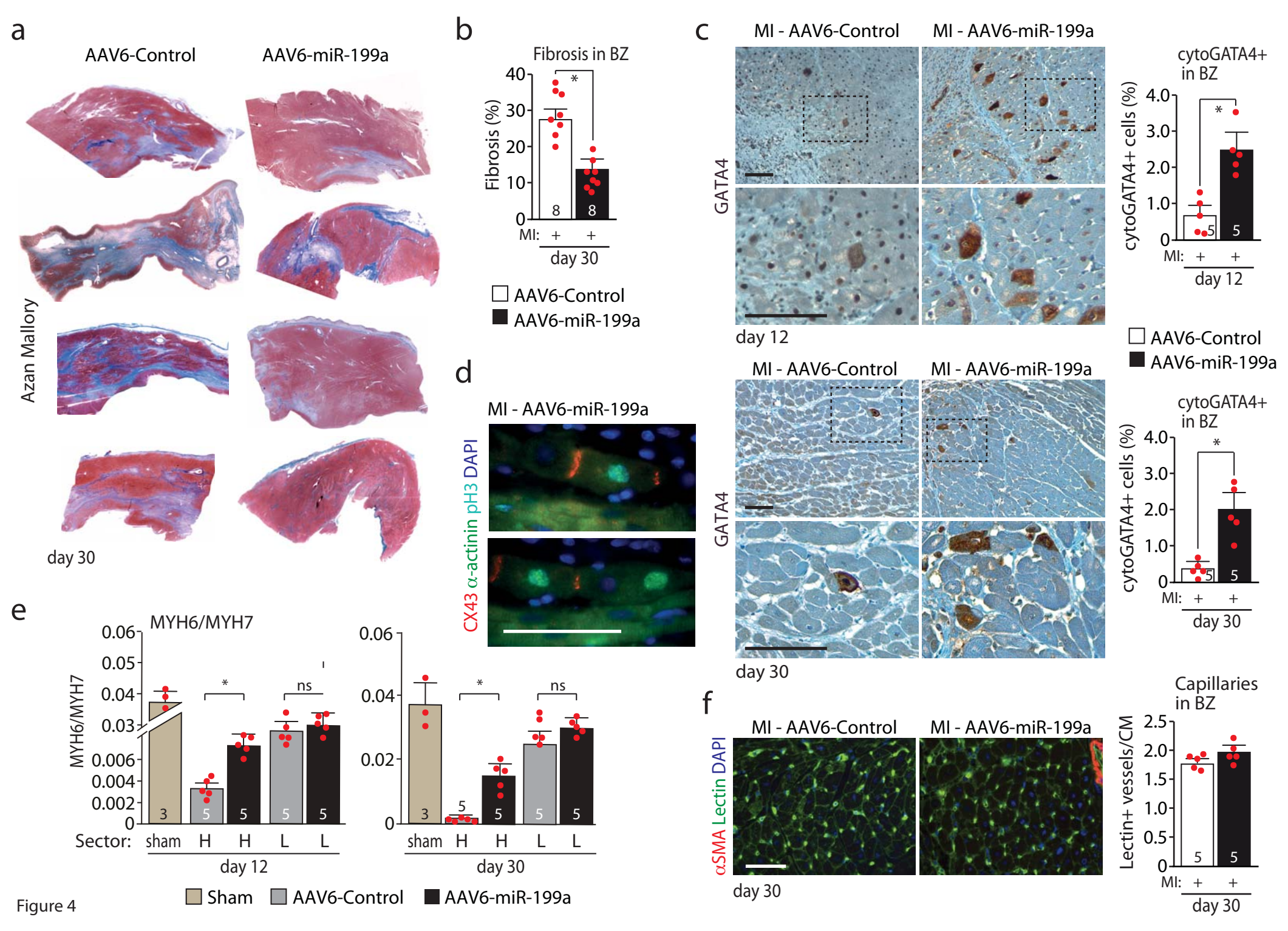
a
AAV6-Control
AAV6-miR-199a
Azan Mallory
day 30
b
Fibrosis in BZ
Fibrosis (%)
MI: + +
day 30
AAV6-Control
AAV6-miR-199a
c
MI - AAV6-Control
MI - AAV6-miR-199a
GATA4
day 12
day 30
cytoGATA4+ in BZ
cytoGATA4+ cells (%)
d
MI - AAV6-miR-199a
CX43 α-actinin pH3 DAPI
e
MYH6/MYH7
Sector: sham H H L L
day 12
day 30
Sham
AAV6-Control
AAV6-miR-199a
f
MI - AAV6-Control
MI - AAV6-miR-199a
αSMA Lectin DAPI
day 30
Capillaries in BZ
Lectin+ vessels/CM

Figure 4

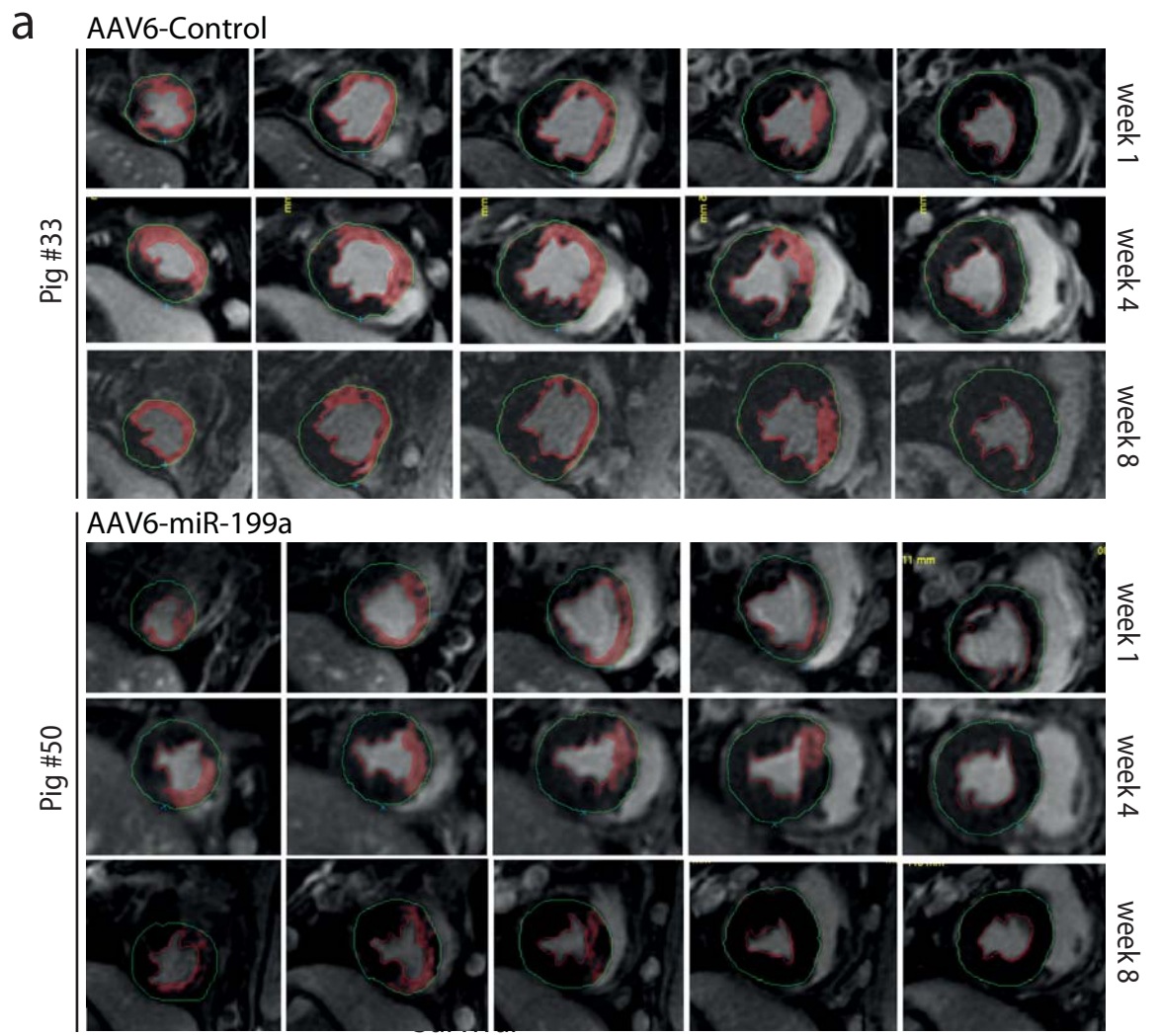

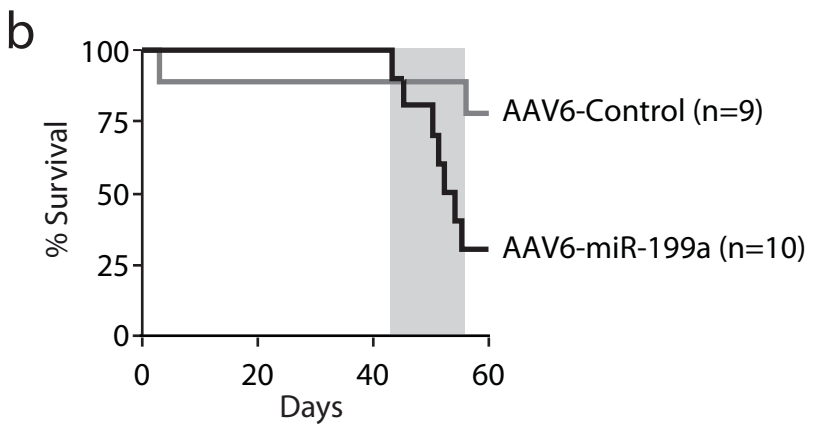

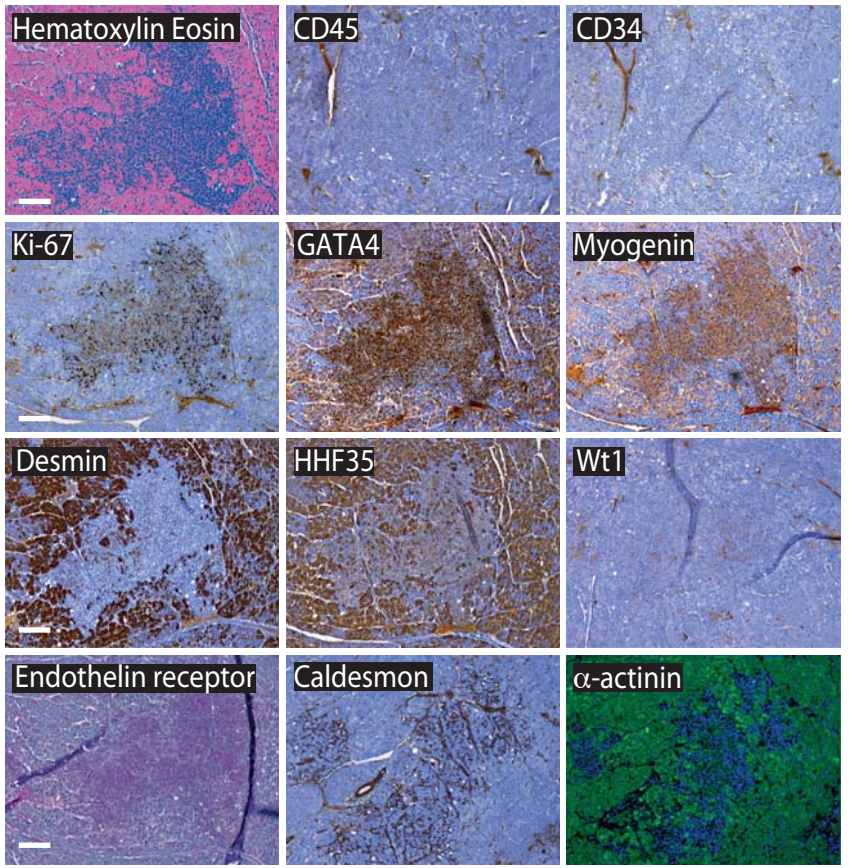

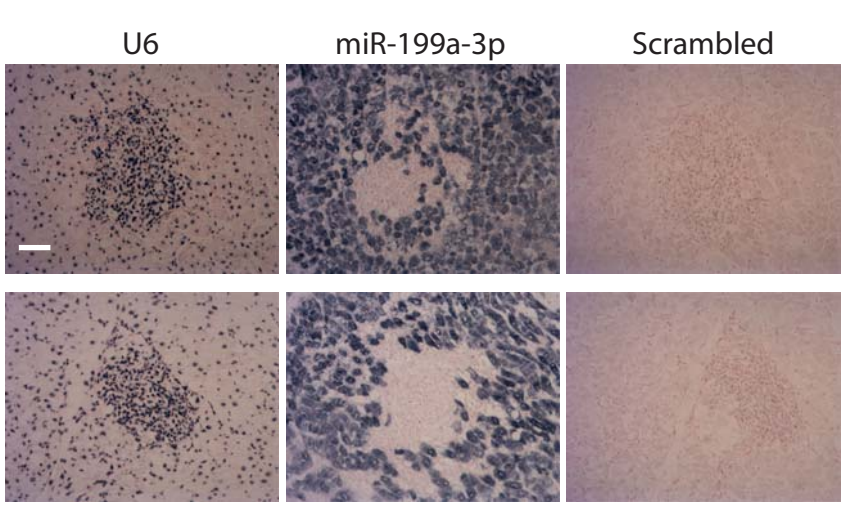

In situ hybridization

Figure 5

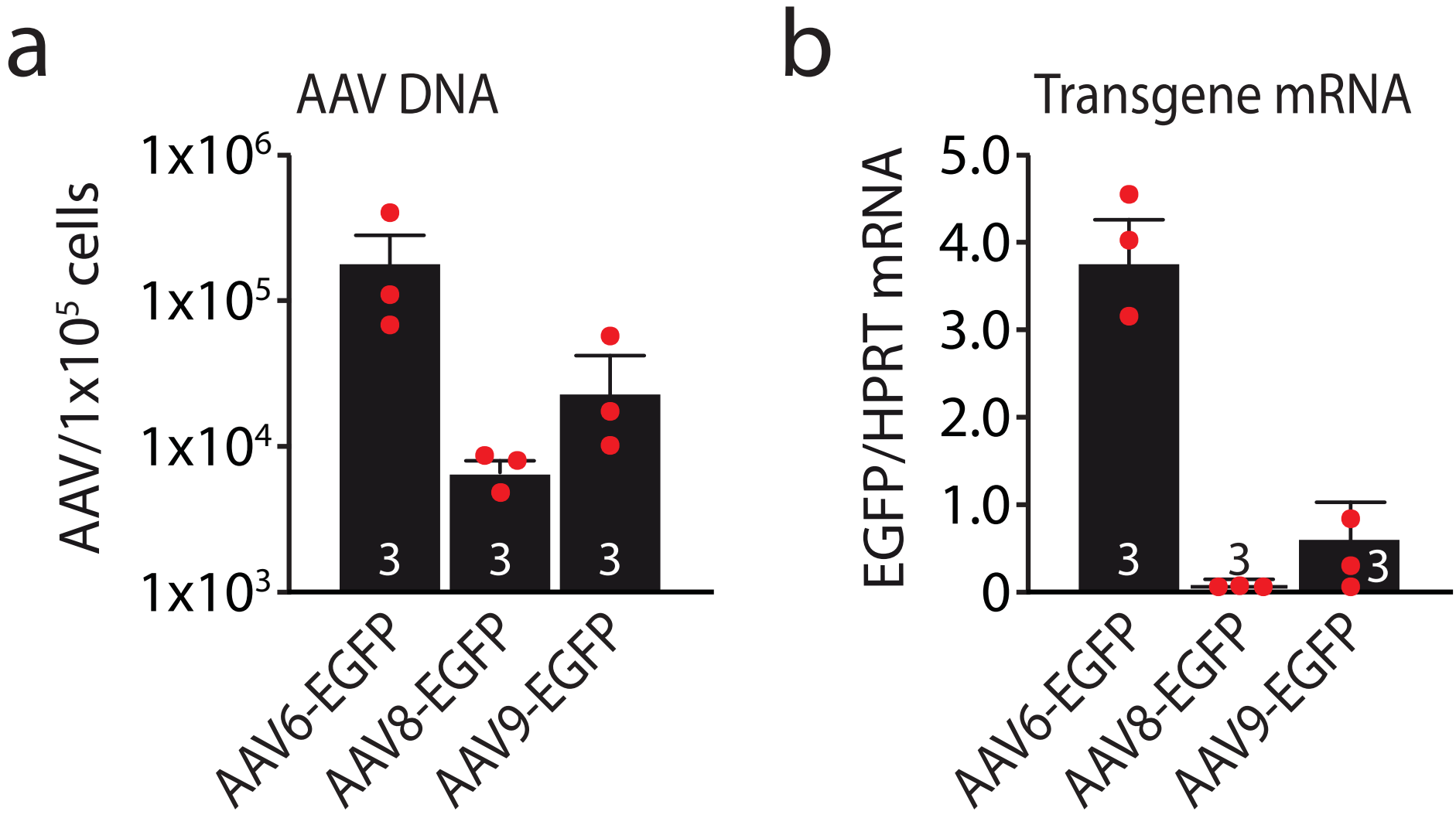
a
AAV DNA
AAV/1x10^5 cells
1x10^6
1x10^5
1x10^4
1x10^3
3
3
3
AAV6-EGFP
AAV8-EGFP
AAV9-EGFP
b
Transgene mRNA
EGFP/HPRT mRNA
5.0
4.0
3.0
2.0
1.0
0
3
3
3
AAV6-EGFP
AAV8-EGFP
AAV9-EGFP

Suppl. Fig. 1

a

Human miR-199a-1 precursor

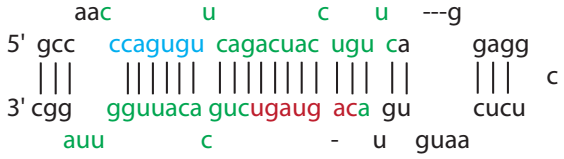

b

	miR-199a-5p
Homo sapiens	cccaguguucagacuaccuguuc
Mus musculus	cccaguguucagacuaccuguuc
Rattus norvegicus	cccaguguucagacuaccuguuc
Sus scrofa	cccaguguucagacuaccuguuc

c

	miR-199a-3p
Homo sapiens	acaguagucugcacauugguua
Mus musculus	acaguagucugcacauugguua
Rattus norvegicus	acaguagucugcacauugguua
Sus scrofa	acaguagucugcacauugguua

Suppl. Fig. 2

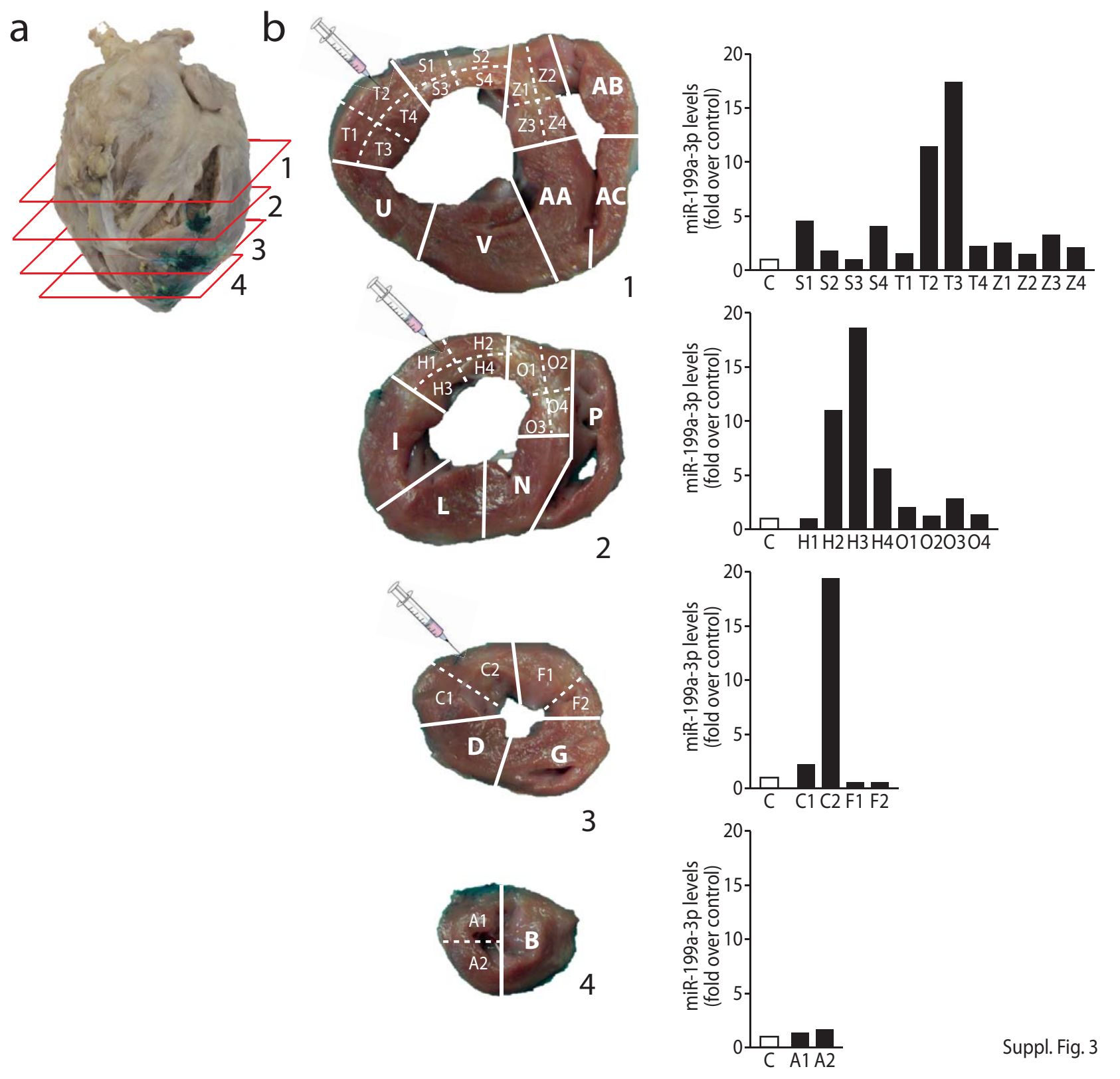
a
b
1
2
3
4
S1
S2
S3
S4
T1
T2
T3
T4
Z1
Z2
Z3
Z4
AB
AA
AC
U
V
H1
H2
H3
H4
O1
O2
O3
O4
I
L
N
P
C1
C2
F1
F2
D
G
A1
A2
B
miR-199a-3p levels
(fold over control)
0
5
10
15
20
C S1 S2 S3 S4 T1 T2 T3 T4 Z1 Z2 Z3 Z4
C H1 H2 H3 H4 O1 O2 O3 O4
C C1 C2 F1 F2
C A1 A2

Suppl. Fig. 3

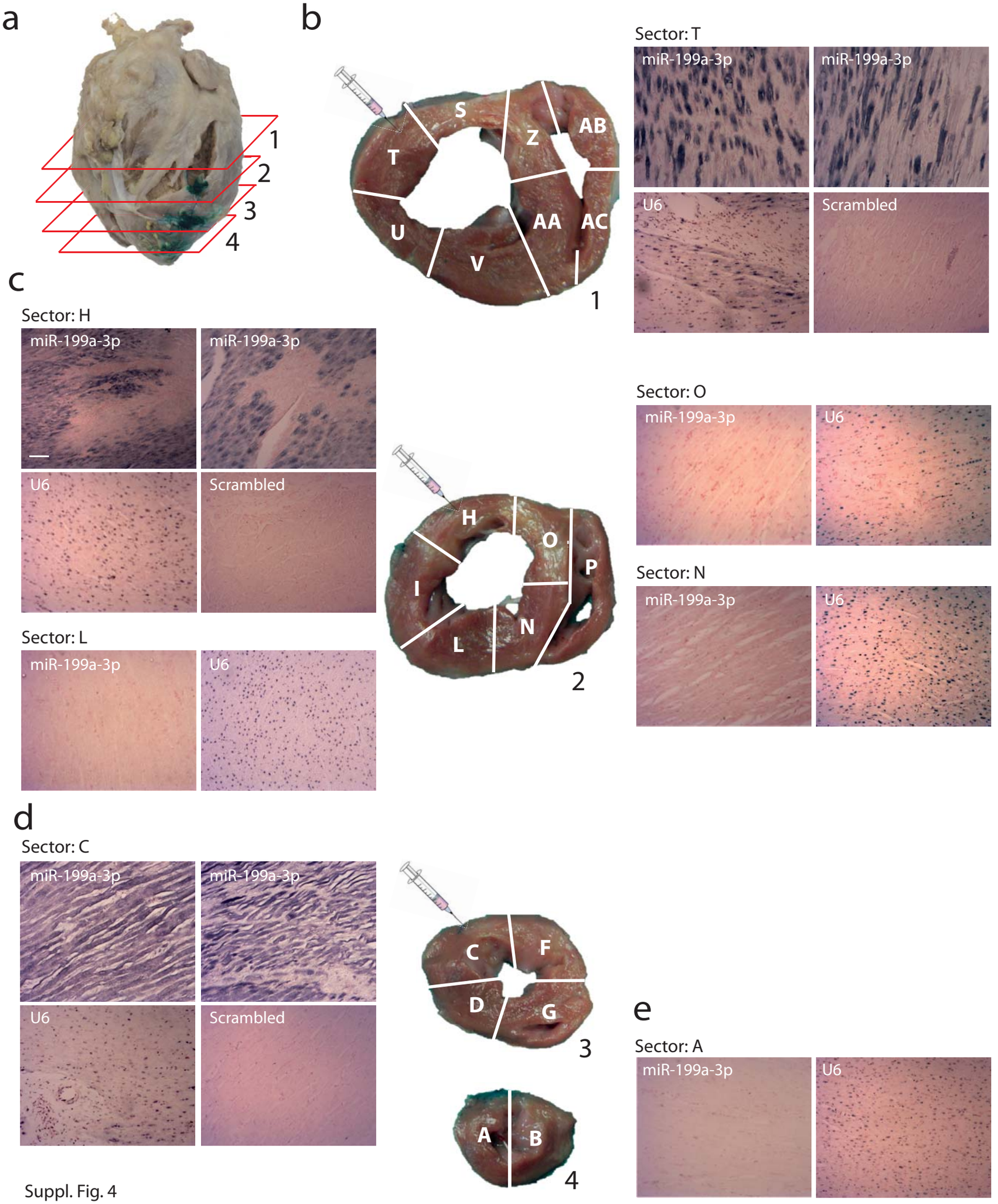
a
1
2
3
4
b
S
Z
AB
T
U
V
AA
AC
1
Sector: T
miR-199a-3p
miR-199a-3p
U6
Scrambled
c
Sector: H
miR-199a-3p
miR-199a-3p
U6
Scrambled
H
O
P
I
N
L
2
Sector: O
miR-199a-3p
U6
Sector: N
miR-199a-3p
U6
Sector: L
miR-199a-3p
U6
d
Sector: C
miR-199a-3p
miR-199a-3p
U6
Scrambled
C
F
D
G
3
A
B
4
e
Sector: A
miR-199a-3p
U6

Suppl. Fig. 4

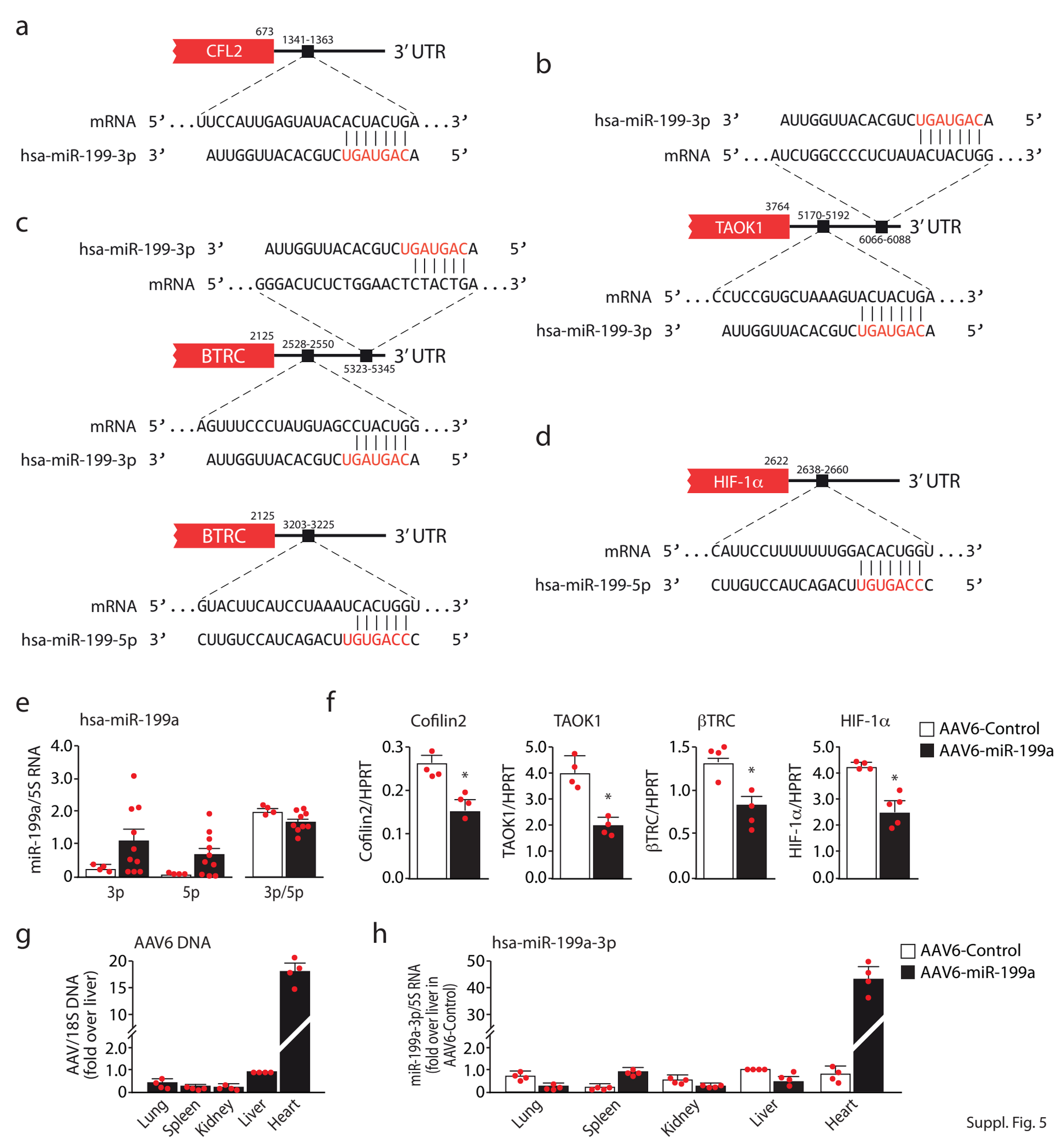
a
CFL2
673
1341-1363
3′ UTR
mRNA 5′...UUCCAUUGAGUAUACACUACUGA...3′
hsa-miR-199-3p 3′ AUUGGUUACACGUCUGAUGACA 5′
b
hsa-miR-199-3p 3′ AUUGGUUACACGUCUGAUGACA 5′
mRNA 5′...AUCUGGCCCCUCUAUACUACUGG...3′
TAOK1
3764
5170-5192
6066-6088
3′ UTR
mRNA 5′...CCUCCGUGCUAAAGUACUACUGA...3′
hsa-miR-199-3p 3′ AUUGGUUACACGUCUGAUGACA 5′
c
hsa-miR-199-3p 3′ AUUGGUUACACGUCUGAUGACA 5′
mRNA 5′...GGGACUCUCTGGAACTCTACTGA...3′
BTRC
2125
2528-2550
5323-5345
3′ UTR
mRNA 5′...AGUUUCCCUAUGUAGCCUACUGG...3′
hsa-miR-199-3p 3′ AUUGGUUACACGUCUGAUGACA 5′
BTRC
2125
3203-3225
3′ UTR
mRNA 5′...GUACUUCAUCCUAAAUCACUGGU...3′
hsa-miR-199-5p 3′ CUUGUCCAUCAGACUUGUGACCC 5′
d
HIF-1α
2622
2638-2660
3′ UTR
mRNA 5′...CAUUCCUUUUUUUGGACACUGGU...3′
hsa-miR-199-5p 3′ CUUGUCCAUCAGACUUGUGACCC 5′
e
hsa-miR-199a
miR-199a/5S RNA
4.0
3.0
2.0
1.0
0
3p
5p
3p/5p
f
Cofilin2
Cofilin2/HPRT
0.3
0.2
0.1
0.0
TAOK1
TAOK1/HPRT
5.0
4.0
3.0
2.0
1.0
0.0
βTRC
βTRC/HPRT
1.5
1.0
0.5
0.0
HIF-1α
HIF-1α/HPRT
5.0
4.0
3.0
2.0
1.0
0.0
*
AAV6-Control
AAV6-miR-199a
g
AAV6 DNA
AAV/18S DNA (fold over liver)
20
15
10
2.0
1.0
0
Lung
Spleen
Kidney
Liver
Heart
h
hsa-miR-199a-3p
miR-199a-3p/5S RNA (fold over liver in AAV6-Control)
50
40
30
2.0
1.0
0
Lung
Spleen
Kidney
Liver
Heart
AAV6-Control
AAV6-miR-199a

Suppl. Fig. 5

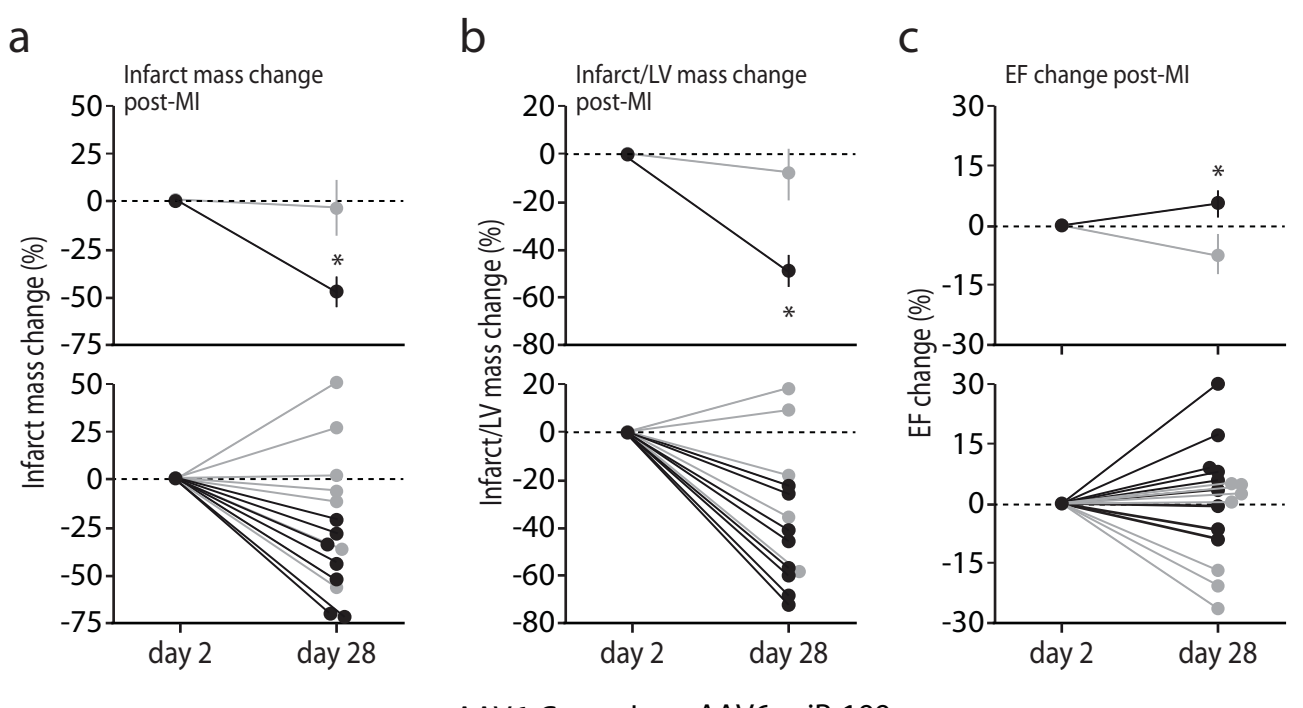
a
Infarct mass change post-MI
Infarct mass change (%)
50
25
0
-25
-50
-75
*
day 2
day 28
b
Infarct/LV mass change post-MI
Infarct/LV mass change (%)
20
0
-20
-40
-60
-80
*
day 2
day 28
c
EF change post-MI
EF change (%)
30
15
0
-15
-30
*
day 2
day 28
AAV6-Control
AAV6-miR-199a

Suppl. Fig. 6

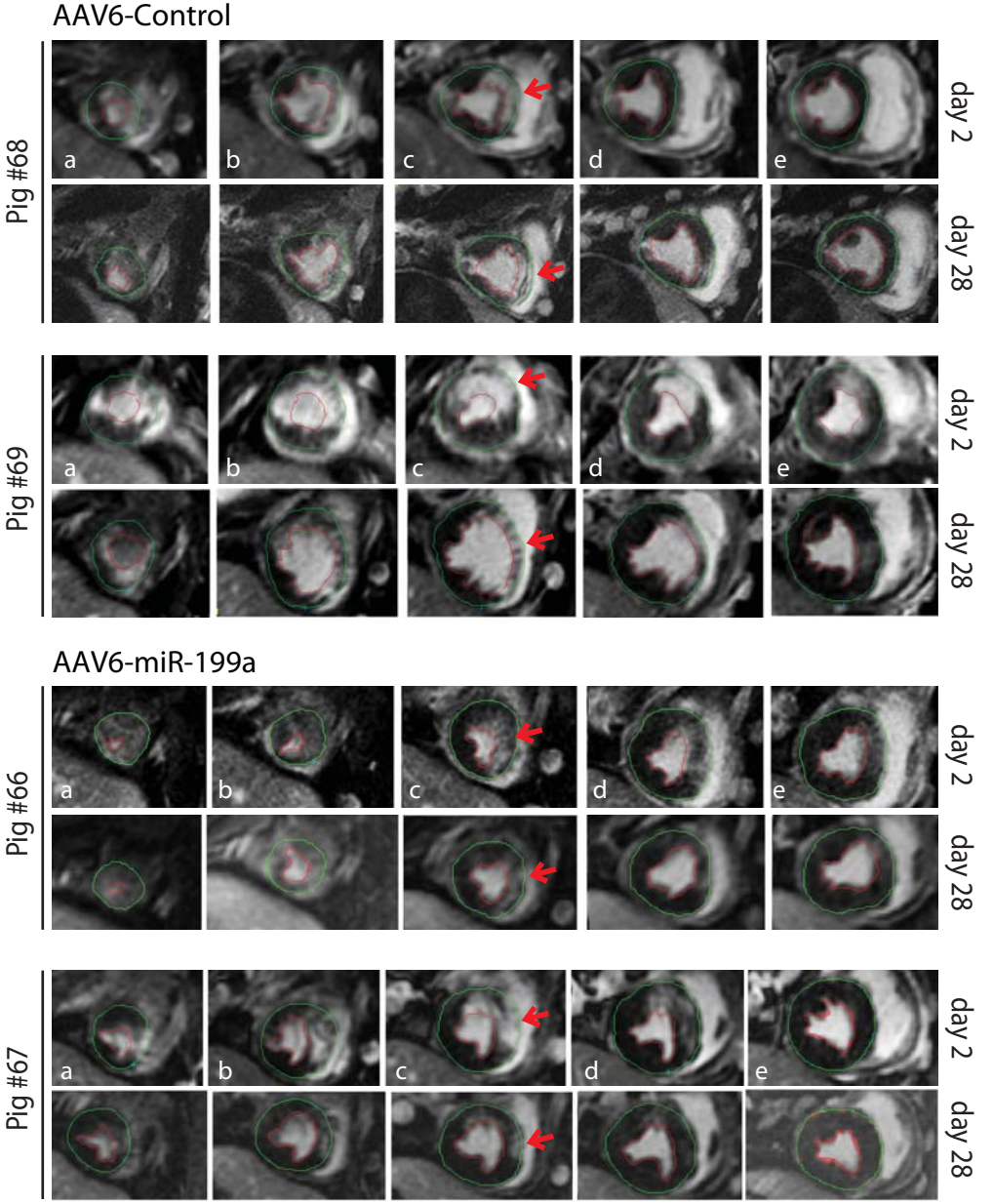
AAV6-Control
Pig #68
Pig #69
AAV6-miR-199a
Pig #66
Pig #67
a
b
c
d
e
day 2
day 28

Suppl. Fig. 7

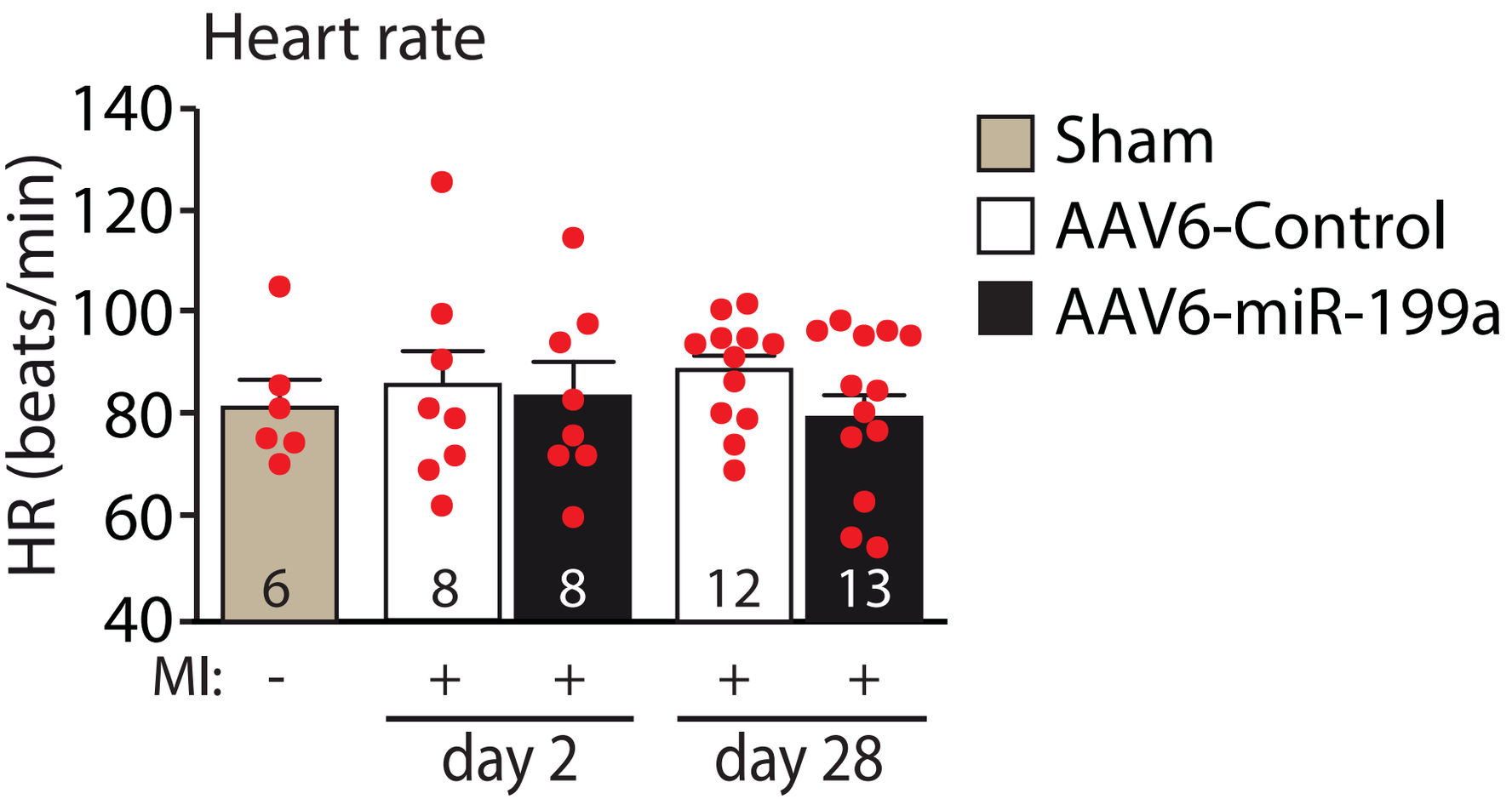
Heart rate
HR (beats/min)
140
120
100
80
60
40
6
8
8
12
13
MI: -
+
+
+
+
day 2
day 28
Sham
AAV6-Control
AAV6-miR-199a

Suppl. Fig. 8

a

Pig #BrdU1 - MI - AAV6-miR-199a - Border zone (sector H)

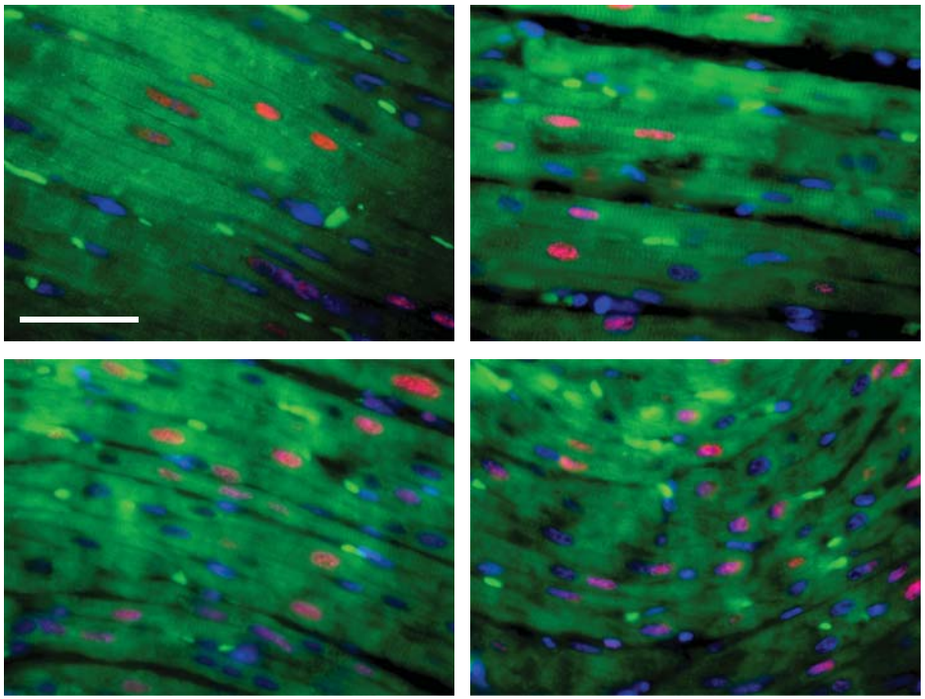

Pig #BrdU1 - MI - AAV6-miR-199a - Remote zone (sector L)

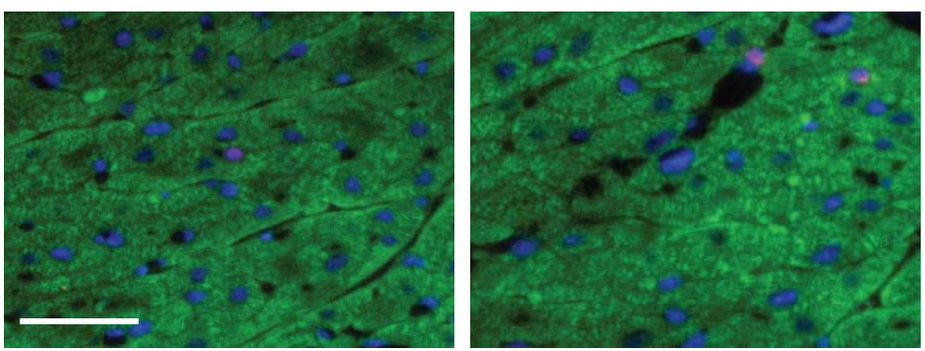

Pig #BrdU4 - MI - AAV6-Control - Border zone (sector H)

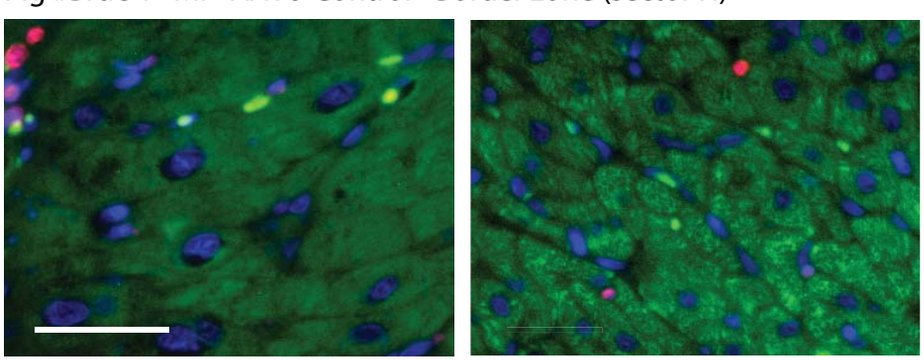

b

4 Different pigs - MI - AAV6-miR-199a - Border zone (sector H)

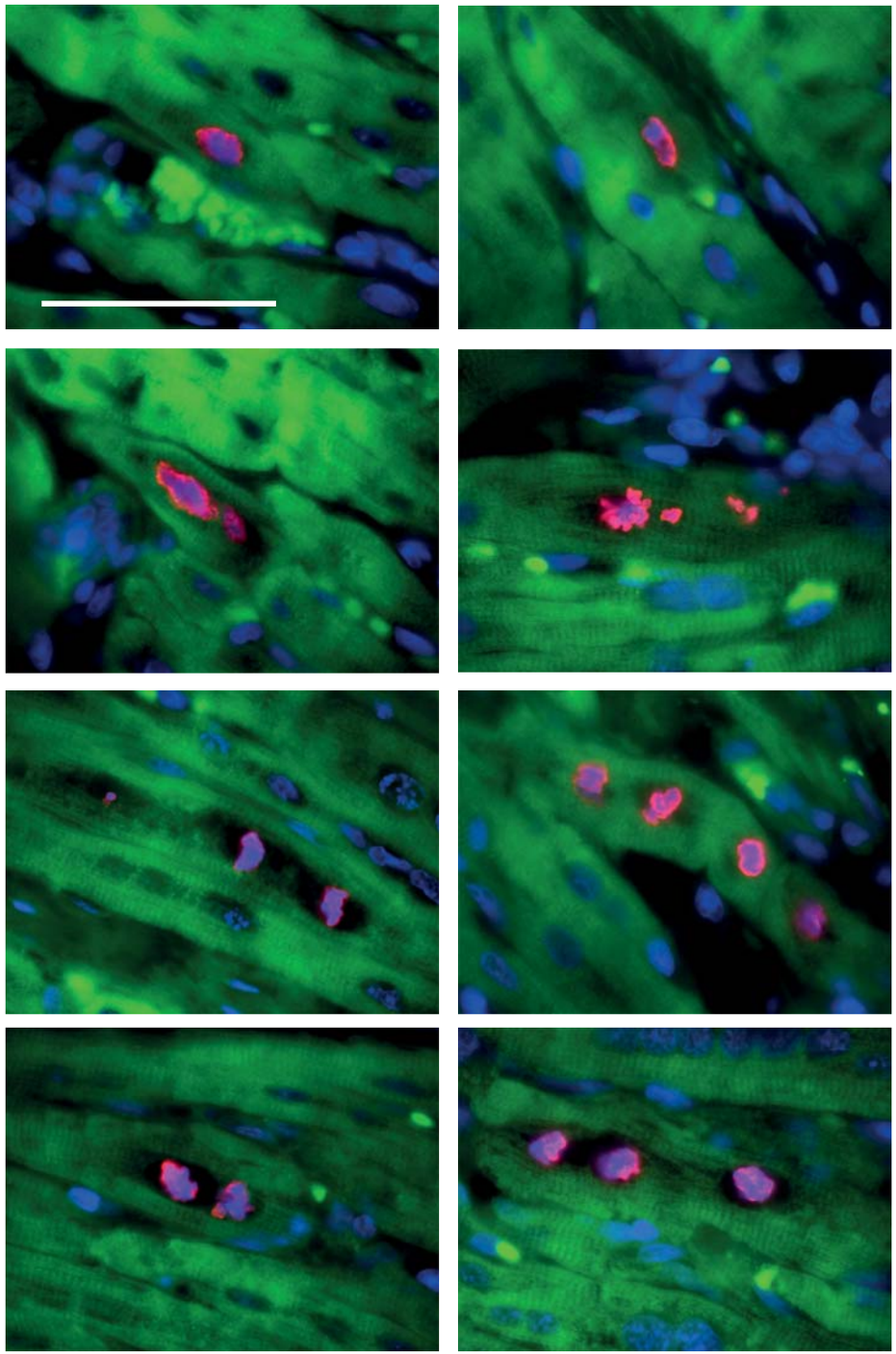

Suppl. Fig. 9

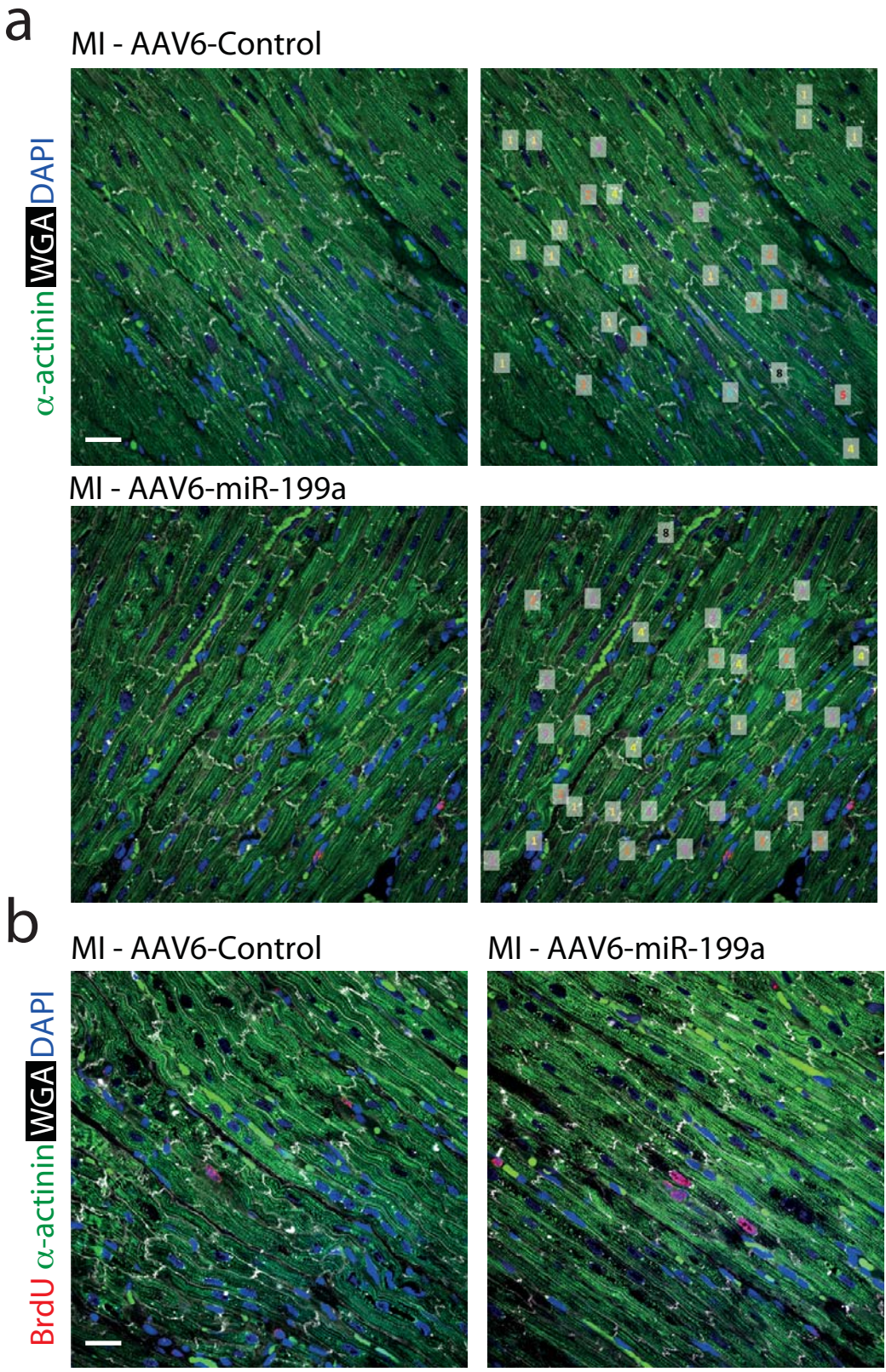
a
MI - AAV6-Control
α-actinin WGA DAPI
MI - AAV6-miR-199a
b
MI - AAV6-Control
MI - AAV6-miR-199a
BrdU α-actinin WGA DAPI

Suppl. Fig. 10

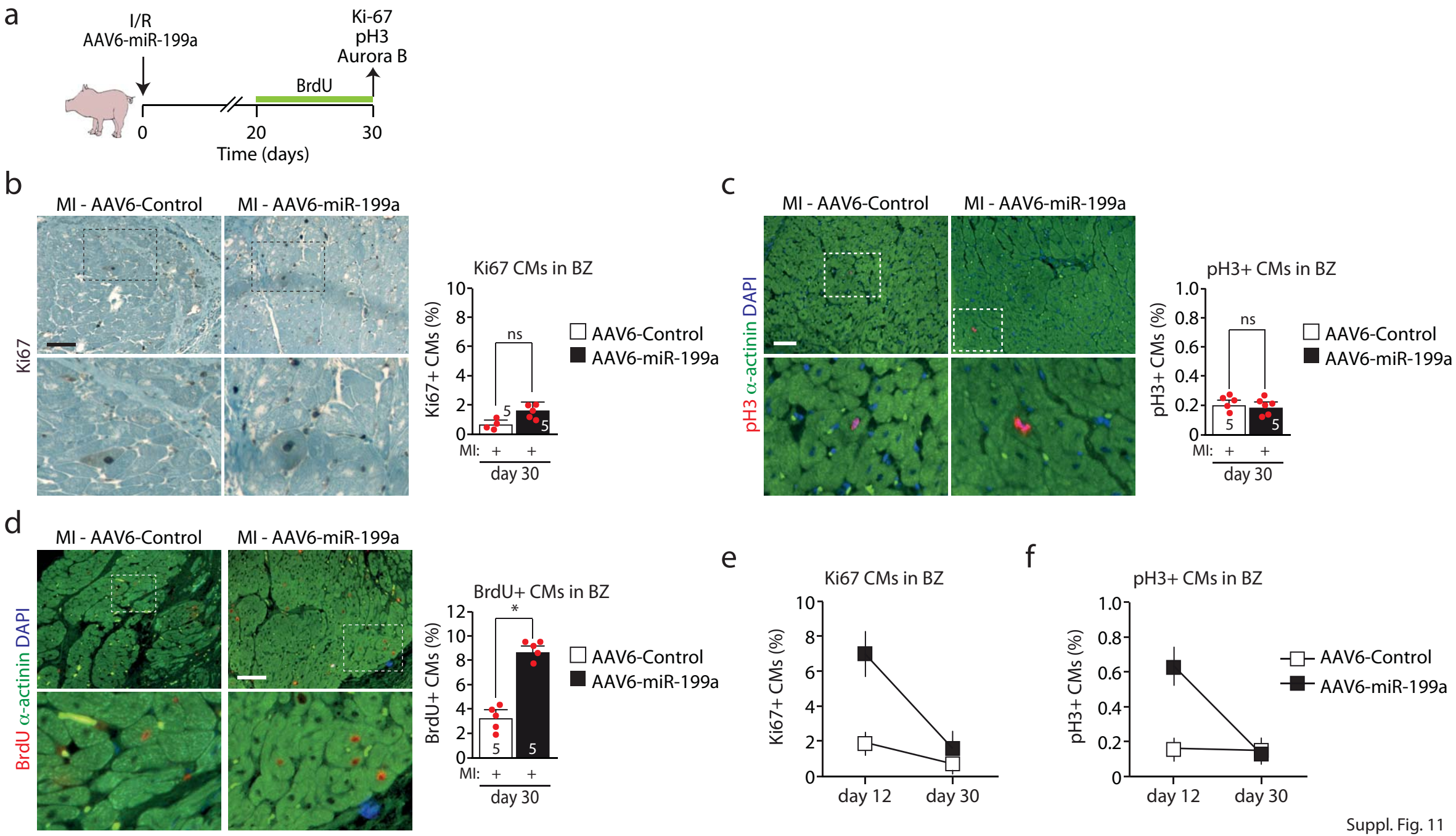
a
I/R
AAV6-miR-199a
Ki-67
pH3
Aurora B
BrdU
0
20
30
Time (days)
b
MI - AAV6-Control
MI - AAV6-miR-199a
Ki67
Ki67 CMs in BZ
Ki67+ CMs (%)
ns
5
5
MI: + +
day 30
AAV6-Control
AAV6-miR-199a
c
MI - AAV6-Control
MI - AAV6-miR-199a
pH3 α-actinin DAPI
pH3+ CMs in BZ
pH3+ CMs (%)
ns
5
5
MI: + +
day 30
AAV6-Control
AAV6-miR-199a
d
MI - AAV6-Control
MI - AAV6-miR-199a
BrdU α-actinin DAPI
BrdU+ CMs in BZ
BrdU+ CMs (%)
*
5
5
MI: + +
day 30
AAV6-Control
AAV6-miR-199a
e
Ki67 CMs in BZ
Ki67+ CMs (%)
day 12
day 30
f
pH3+ CMs in BZ
pH3+ CMs (%)
day 12
day 30
AAV6-Control
AAV6-miR-199a

Suppl. Fig. 11

Pig #BrdU1 - MI -AAV6-miR-199a
Border zone (sector H)

Remote (sector L)

Pig #BrdU4 - MI -AAV6-Control
Border zone (sector H)

GATA4

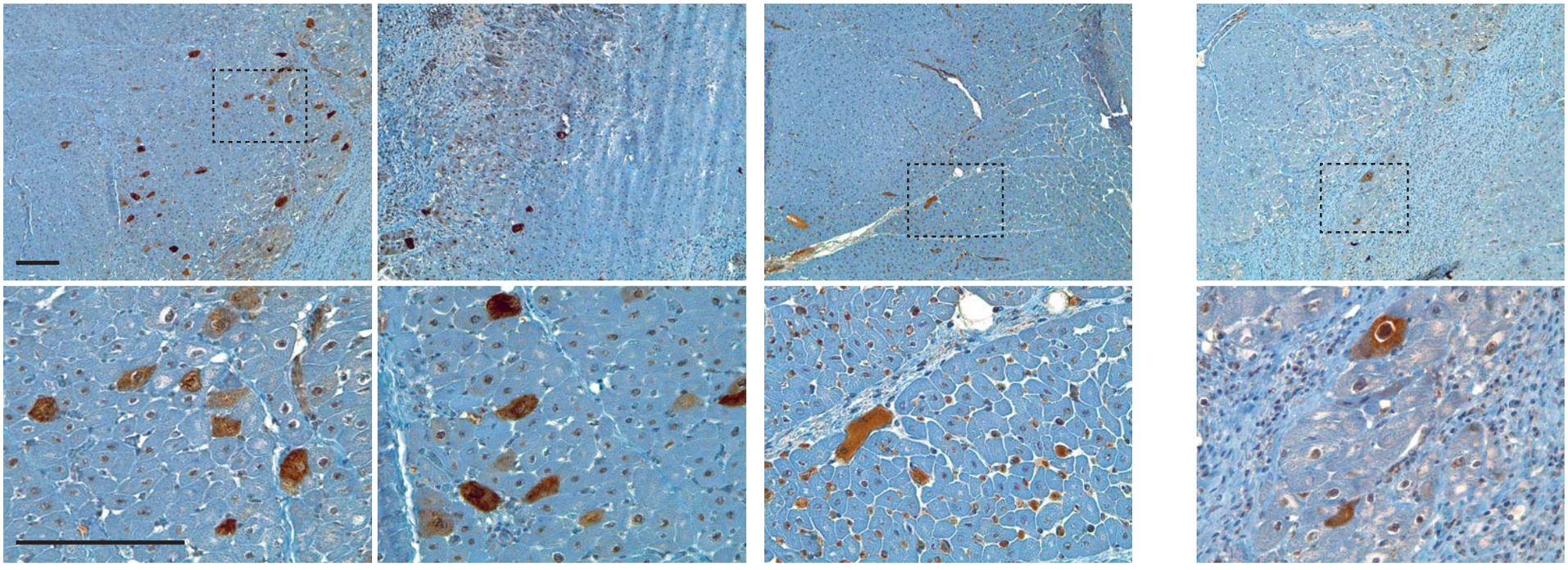

12 days

Pig #MAI1 - MI -AAV6-miR-199a
Border zone (sector H)

Remote (sector L)

Pig #ADD6 - MI -AAV7-Control
Border zone (sector H)

GATA4

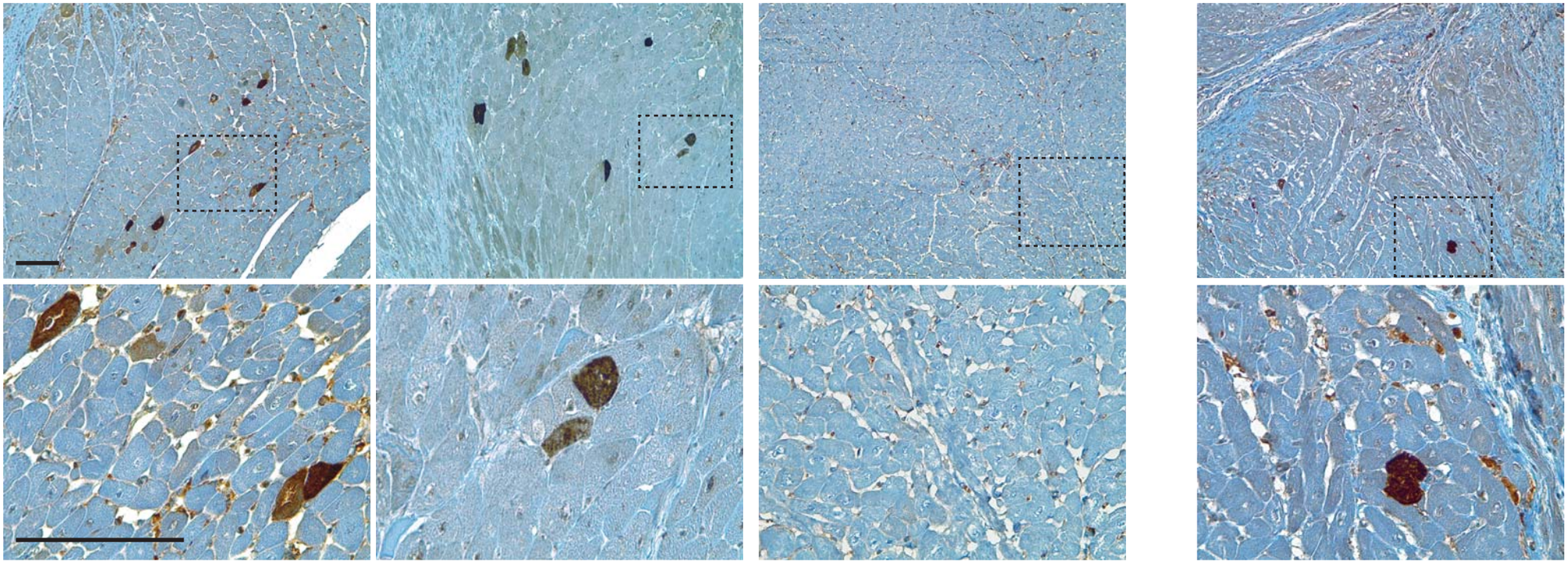

30 days

Suppl. Fig. 12

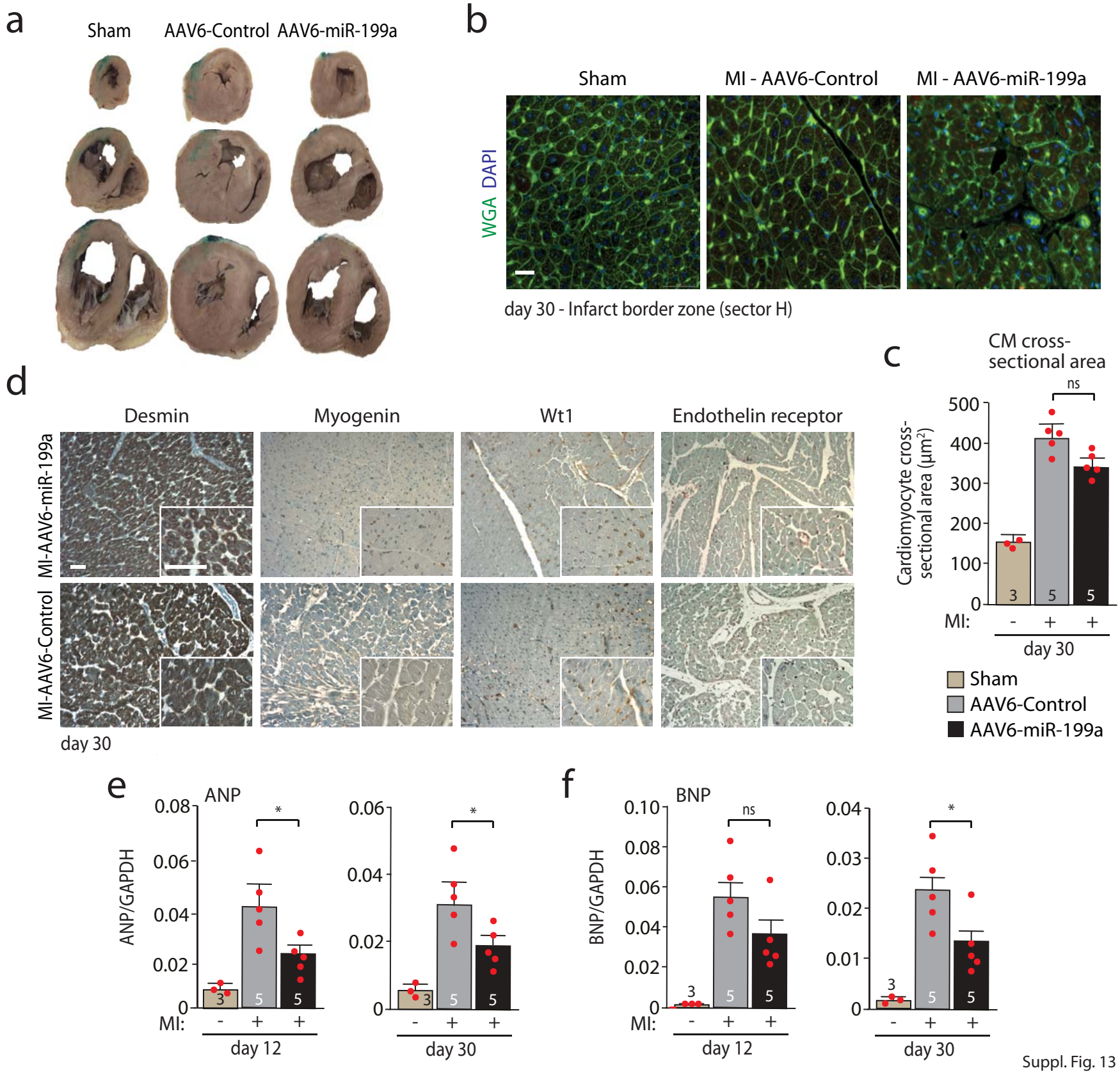
a
Sham
AAV6-Control
AAV6-miR-199a
b
Sham
MI - AAV6-Control
MI - AAV6-miR-199a
WGA DAPI
day 30 - Infarct border zone (sector H)
c
CM cross-sectional area
ns
Cardiomyocyte cross-sectional area (µm²)
500
400
300
200
100
0
3
5
5
MI:
-
+
+
day 30
Sham
AAV6-Control
AAV6-miR-199a
d
Desmin
Myogenin
Wt1
Endothelin receptor
MI-AAV6-miR-199a
MI-AAV6-Control
day 30
e
ANP
ANP/GAPDH
0.08
0.06
0.04
0.02
0
*
3
5
5
MI:
-
+
+
day 12
0.06
0.04
0.02
0
*
day 30
f
BNP
BNP/GAPDH
0.10
0.08
0.06
0.04
0.02
0
ns
day 12
0.04
0.03
0.02
0.01
0
*
day 30

Suppl. Fig. 13

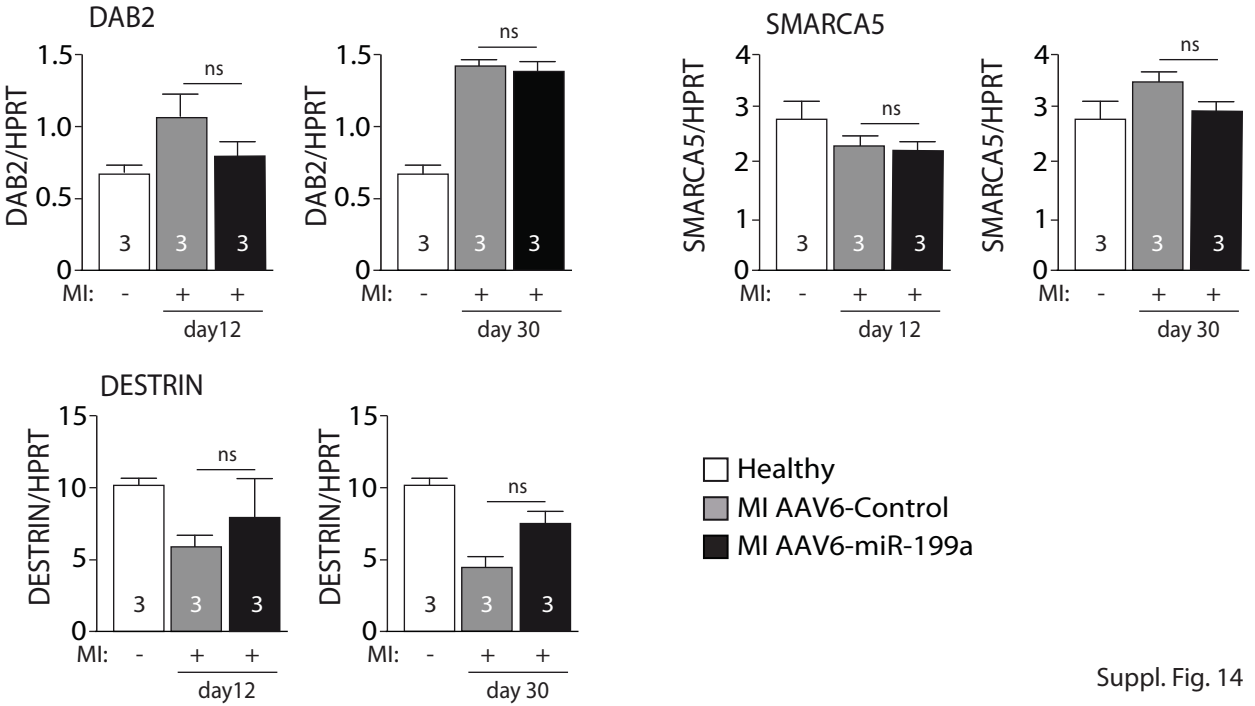
DAB2
DAB2/HPRT
1.5
1.0
0.5
0
ns
3
3
3
MI: - + +
day12
DAB2/HPRT
1.5
1.0
0.5
0
ns
3
3
3
MI: - + +
day 30
SMARCA5
SMARCA5/HPRT
4
3
2
1
0
ns
3
3
3
MI: - + +
day 12
SMARCA5/HPRT
4
3
2
1
0
ns
3
3
3
MI: - + +
day 30
DESTRIN
DESTRIN/HPRT
15
10
5
0
ns
3
3
3
MI: - + +
day12
DESTRIN/HPRT
15
10
5
0
ns
3
3
3
MI: - + +
day 30
Healthy
MI AAV6-Control
MI AAV6-miR-199a

Suppl. Fig. 14

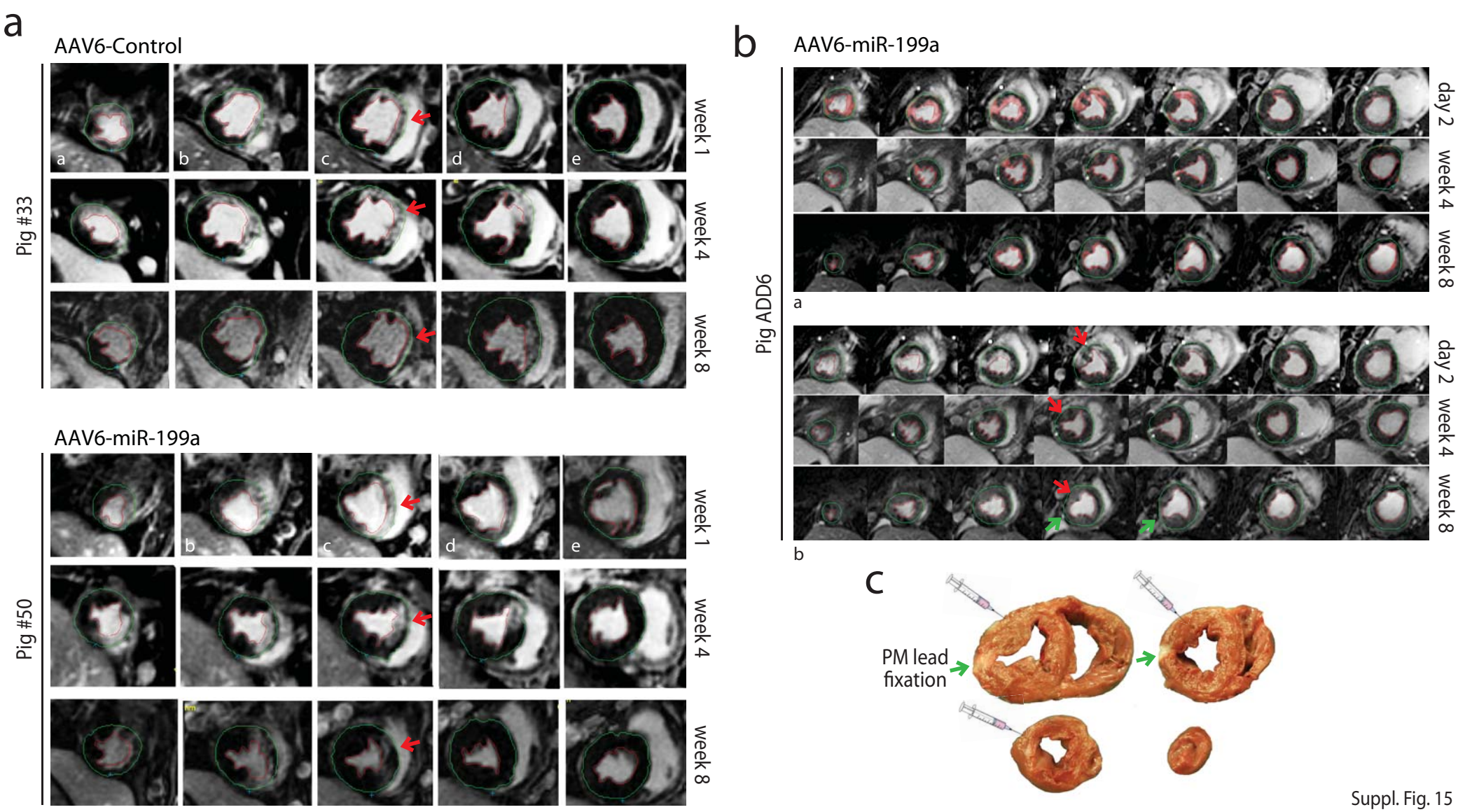
a
AAV6-Control
Pig #33
week 1
week 4
week 8
AAV6-miR-199a
Pig #50
week 1
week 4
week 8
b
AAV6-miR-199a
Pig ADD6
day 2
week 4
week 8
a
day 2
week 4
week 8
b
c
PM lead
fixation

Suppl. Fig. 15

a

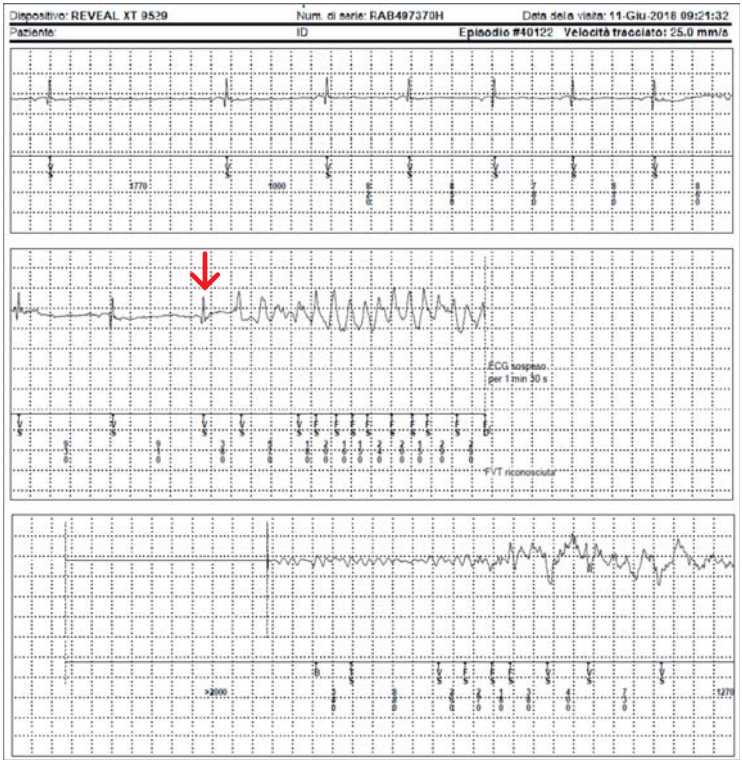

b

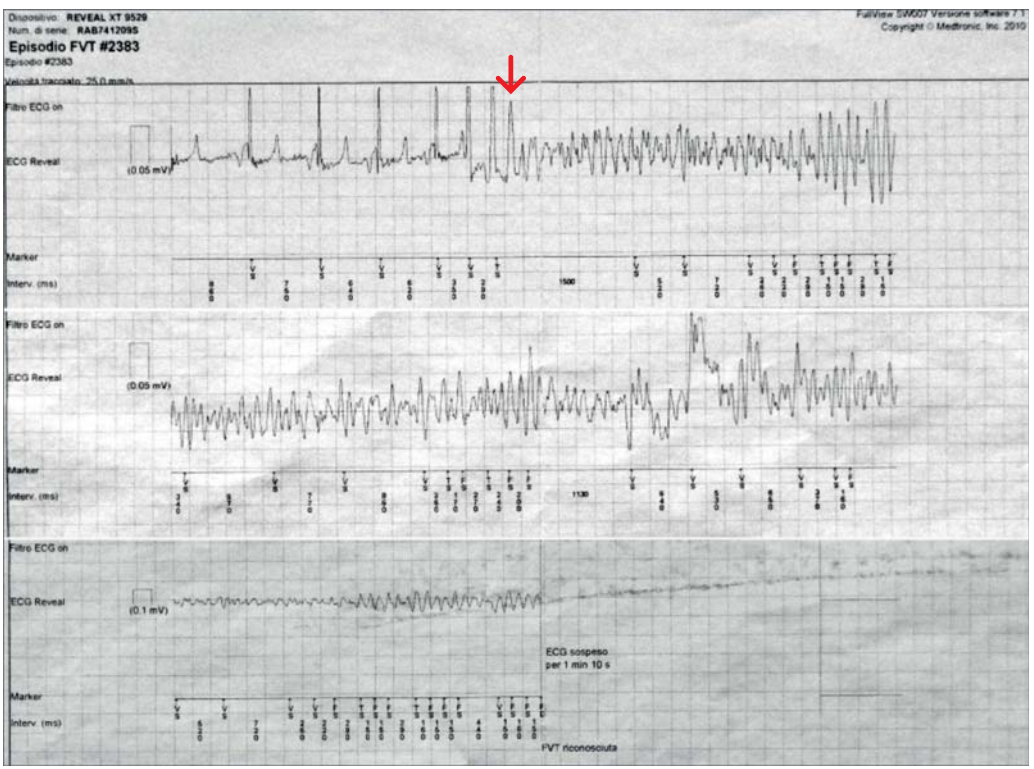

Suppl. Fig. 16

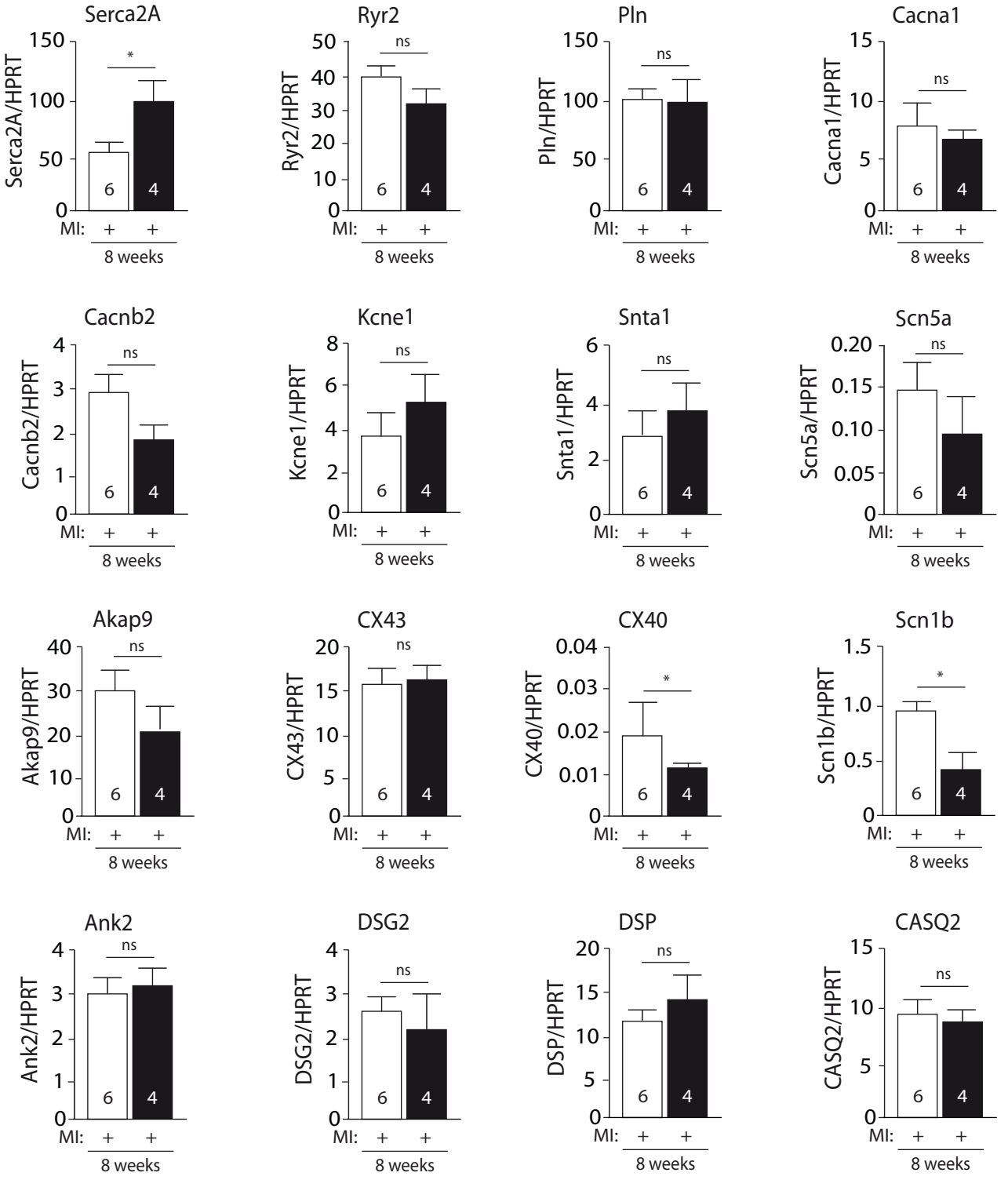
Serca2A
Serca2A/HPRT
150
100
50
0
*
6
4
MI: + +
8 weeks
Ryr2
Ryr2/HPRT
50
40
30
20
10
0
ns
6
4
MI: + +
8 weeks
Pln
Pln/HPRT
150
100
50
0
ns
6
4
MI: + +
8 weeks
Cacna1
Cacna1/HPRT
15
10
5
0
ns
6
4
MI: + +
8 weeks
Cacnb2
Cacnb2/HPRT
4
3
2
1
0
ns
6
4
MI: + +
8 weeks
Kcne1
Kcne1/HPRT
8
6
4
2
0
ns
6
4
MI: + +
8 weeks
Snta1
Snta1/HPRT
6
4
2
0
ns
6
4
MI: + +
8 weeks
Scn5a
Scn5a/HPRT
0.20
0.15
0.10
0.05
0
ns
6
4
MI: + +
8 weeks
Akap9
Akap9/HPRT
40
30
20
10
0
ns
6
4
MI: + +
8 weeks
CX43
CX43/HPRT
20
15
10
5
0
ns
6
4
MI: + +
8 weeks
CX40
CX40/HPRT
0.04
0.03
0.02
0.01
0
*
6
4
MI: + +
8 weeks
Scn1b
Scn1b/HPRT
1.5
1.0
0.5
0
*
6
4
MI: + +
8 weeks
Ank2
Ank2/HPRT
4
3
2
1
0
ns
6
4
MI: + +
8 weeks
DSG2
DSG2/HPRT
4
3
2
1
0
ns
6
4
MI: + +
8 weeks
DSP
DSP/HPRT
20
15
10
5
0
ns
6
4
MI: + +
8 weeks
CASQ2
CASQ2/HPRT
15
10
5
0
ns
6
4
MI: + +
8 weeks
AAV6-Control
AAV6-miR-199a

Suppl. Fig. 17

Hematoxylin Eosin

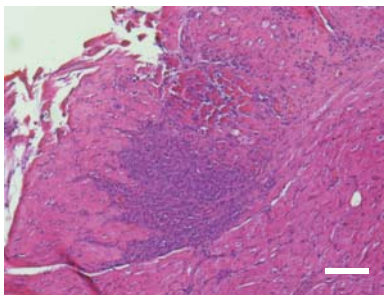
Pig #27, MI, 4 weeks, I

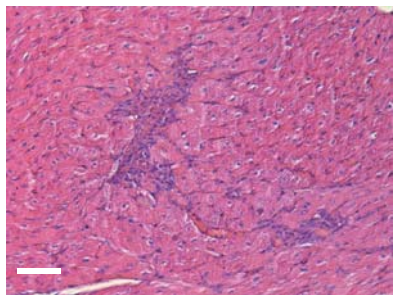
Pig #27, MI, 4 weeks, I

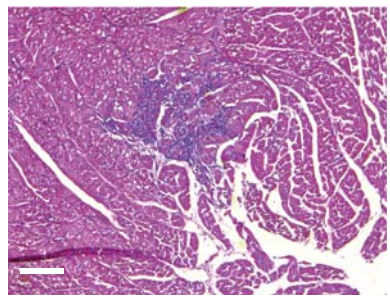
Pig #27, MI, 4 weeks, H

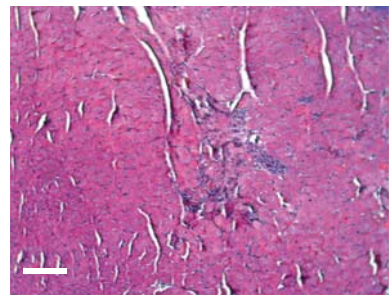
Pig #ADD2, no MI, 12 days, H

α-actinin, Hoeschst

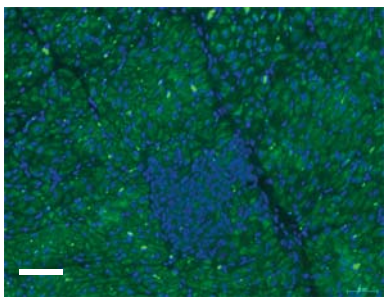
Pig #50, MI, 8 weeks, T

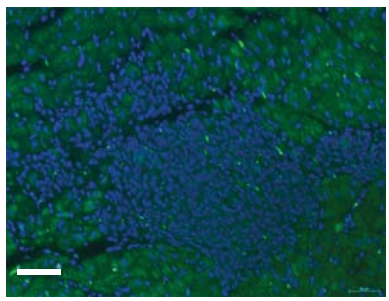
Pig #50, MI, 8 weeks, T

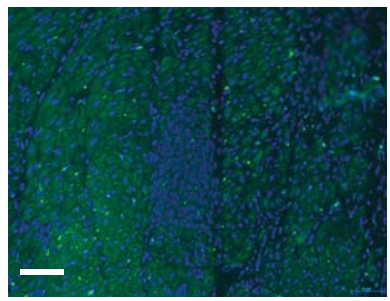
Pig #50, MI, 8 weeks, U

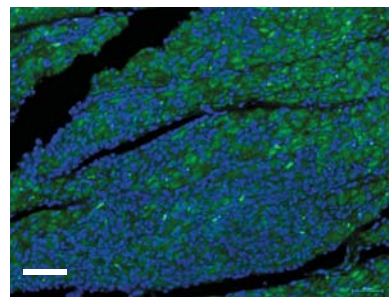
Pig #50, MI, 8 weeks, T

Ki67

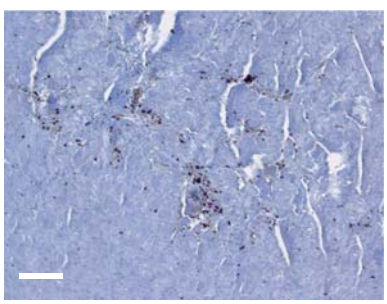
Pig #ADD2, no MI, 12 days, H

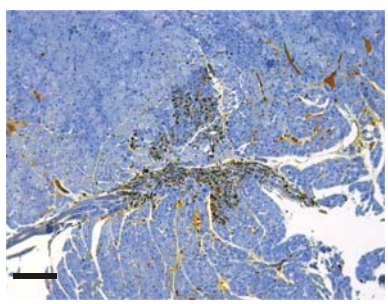
Pig #27, MI, 4 weeks, H

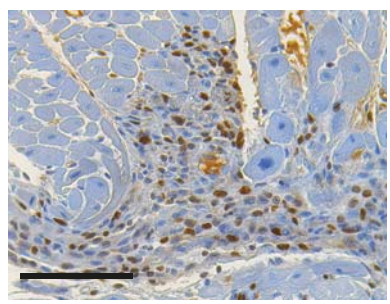
Pig #27, MI, 4 weeks, H

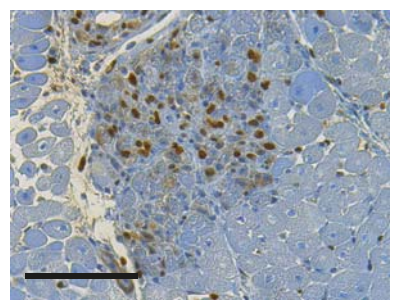
Pig #27, MI, 4 weeks, H

GATA4

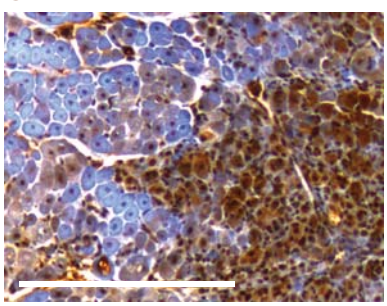
Pig #50 MI, 8 weeks, H

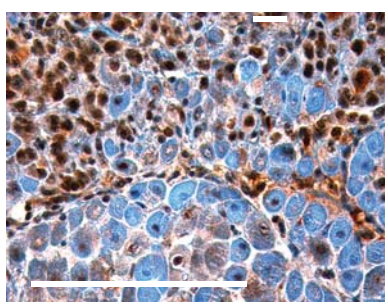
Pig #50 MI, 8 weeks, H

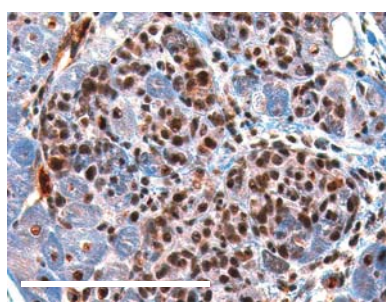
Pig #50 MI, 8 weeks, H

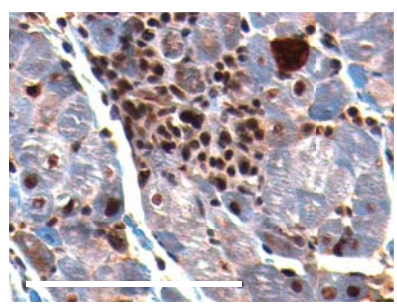
Pig #50 MI, 8 weeks, H

Myogenin

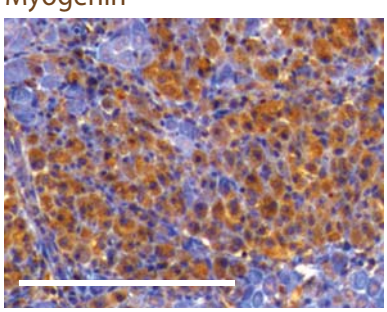
Pig #50 MI, 8 weeks, H

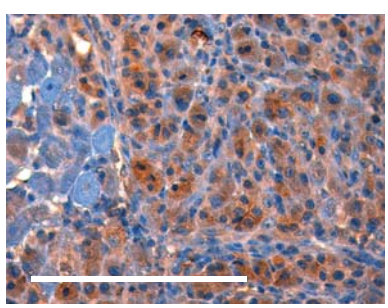
Pig #50 MI, 8 weeks, H

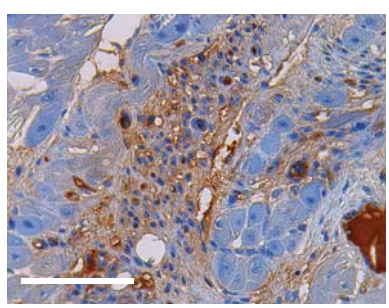
Pig #50 MI, 8 weeks, H

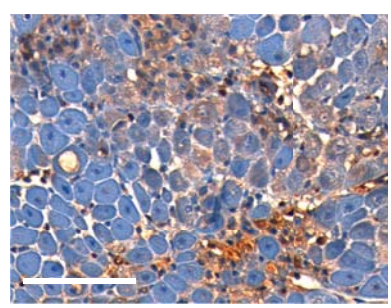
Pig #50 MI, 8 weeks, H

Suppl. Fig. 18

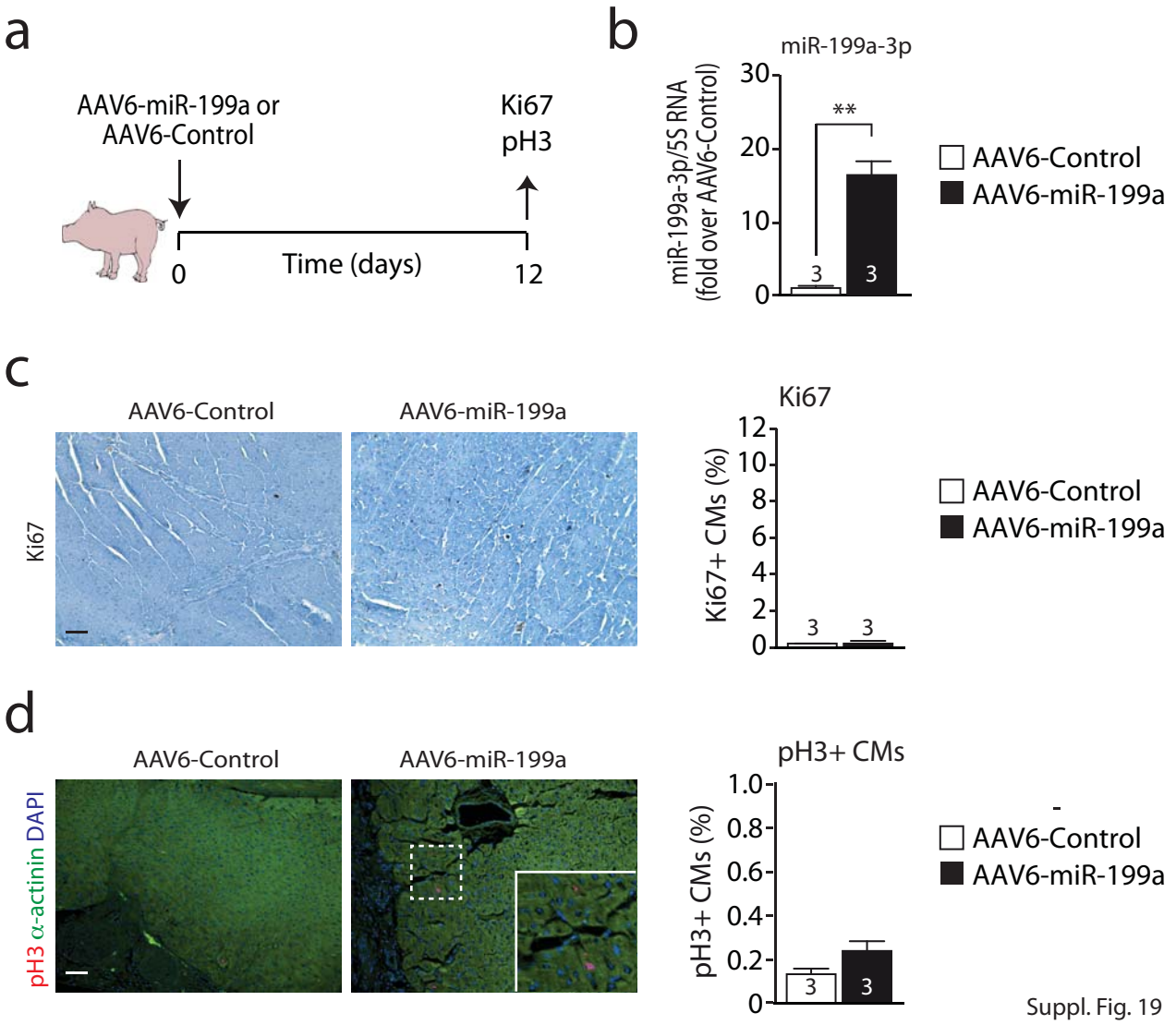
a
AAV6-miR-199a or
AAV6-Control
Ki67
pH3
0
Time (days)
12
b
miR-199a-3p
miR-199a-3p/5S RNA
(fold over AAV6-Control)
30
20
10
0
**
3
3
AAV6-Control
AAV6-miR-199a
c
AAV6-Control
AAV6-miR-199a
Ki67
Ki67
Ki67+ CMs (%)
12
10
8
6
4
2
0
3
3
AAV6-Control
AAV6-miR-199a
d
AAV6-Control
AAV6-miR-199a
pH3 α-actinin DAPI
pH3+ CMs
pH3+ CMs (%)
1.0
0.8
0.6
0.4
0.2
0
3
3
AAV6-Control
AAV6-miR-199a

Suppl. Fig. 19

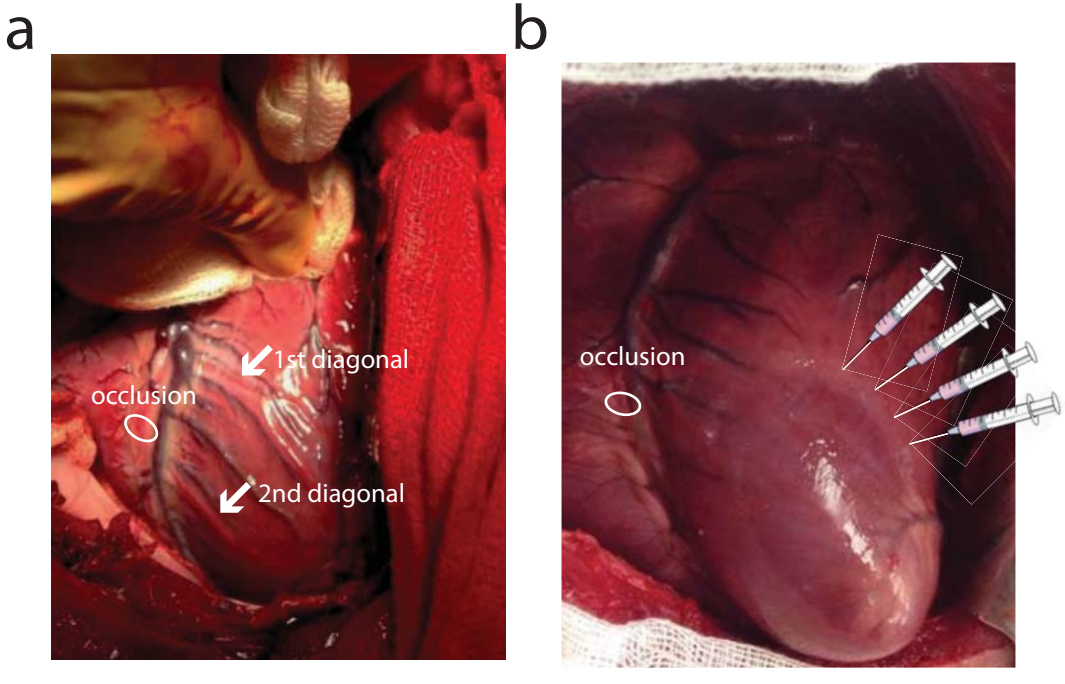

Suppl. Fig. 20

Supplementary Table I. Functional and morphological parameters from cMRI analyses.

Day 2							
AAV6-Control	EDV (ml)	ESV (ml)	SV (ml)	EF (%)	scar (g)	LV mass (g)	scar (%)
1 Pig 43	39.65	14.87	25.00	63.05	9.00	47.90	18.79
2 Pig 46	62.20	24.00	38.20	61.41	13.06	57.72	22.63
3 Pig 51	65.36	23.94	41.42	63.37	12.57	48.27	26.04
4 Pig 52	57.32	20.78	36.54	63.74	14.92	63.39	23.53
5 Pig 68	58.00	21.80	36.20	62.41	7.94	50.59	15.69
6 ADD 03	61.11	19.45	41.66	68.17	5.10	52.03	9.80
7 ADD 07	71.18	27.92	43.26	60.77	23.40	69.56	33.64
8 ADD 13	70.82	27.15	43.67	61.66	13.82	70.67	19.56
Mean	60.70	22.49	38.24	63.07635	12.48	57.52	21.21
Day 28							
AAV6-Control	EDV (ml)	ESV (ml)	SV (ml)	EF (%)	scar (g)	LV mass (g)	scar (%)
1 Pig 43	62.77	21.15	41.62	66.30	13.51	60.86	22.20
2 Pig 46	72.17	29.50	42.67	59.12	13.24	68.00	19.47
3 Pig 51	77.02	25.55	51.47	66.83	11.67	54.61	21.37
4 Pig 52	94.63	50.26	44.37	46.89	15.23	59.11	25.77
5 Pig 68	61.10	22.10	39.00	63.83	10.05	58.48	17.19
6 ADD 03	67.89	21.45	46.44	68.40	2.2	53.04	4.15
7 ADD 07	97.79	48.35	49.44	50.58	14.89	68.57	21.72
8 ADD 13	119.94	61.37	58.57	48.83	13.43	62.68	21.43
9 Pig 25	128.42	80.03	48.39	37.68	19	63.45	29.94
10 Pig 29	82.07	41.35	40.72	49.62	23.94	79.30	30.19
11 Pig 33	96.77	55.17	41.60	42.99	18.6	99.78	18.64
12 Pig 34	96.08	44.04	52.04	54.16	5.72	70.96	8.06
Mean	88.05	41.70	46.36	54.60	13.46	66.57	20.01

%

Suppl. Table I continued

Day 2							
AAV6-miR-199a	EDV (ml)	ESV (ml)	SV (ml)	EF (%)	scar (g)	LV mass (g)	scar (%)
1 Pig 54	69.15	30.59	38.56	55.76	18.52	54.19	34.18
2 Pig 55	60.10	28.37	31.73	52.79	10.38	59.96	17.32
3 Pig 66	64.18	20.71	43.46	67.72	14.17	58.66	24.16
4 Pig 67	73.17	23.98	49.19	67.23	10.62	61.15	17.37
5 Pig 69	49.40	17.02	32.38	65.55	14.76	51.21	28.82
6 ADD 05	70.20	19.74	50.68	72.19	7.21	53.59	13.45
7 ADD 06	57.64	20.56	37.07	64.31298	10.8	64.36	16.78
8 ADD 16	57.75	27.56	30.19	52.27706	16.08	63.7	25.24
Mean	62.70	23.57	39.16	62.23	12.82	58.35	22.16

Day 28							
AAV6-miR-199a	EDV (ml)	ESV (ml)	SV (ml)	EF (%)	scar (g)	LV mass (g)	scar (%)
1 Pig 54	76.00	33.85	42.15	55.46	12.35	61.35	20.13
2 Pig 55	97.16	34.15	63.01	64.85	8.20	63.73	12.87
3 Pig 66	65.81	18.7	47.11	71.58	3.98	51.4	7.74
4 Pig 67	85.44	23.48	61.96	72.52	6.00	64.00	9.37
5 Pig 69	68.98	26.73	42.25	61.25	7.21	57.80	12.47
6 ADD 05	72.00	18.34	53.66	74.53	3.49	64.64	5.40
7 ADD 06	66.42	19.96	46.46	69.95	3.20	66.20	4.83
8 ADD 16	92.67	48.51	44.16	47.65	11.72	60.02	19.53
9 Pig 21	62.92	16.76	46.16	73.36	4.88	69.40	7.03
10 Pig 26	80.43	29.84	50.59	62.90	6.60	65.39	10.09
11 Pig 27	92.40	32.99	59.41	64.30	5.99	59.70	10.03
12 Pig 32	78.44	33.29	45.15	57.56	11.40	69.50	16.40
13 Pig 50	76.83	25.15	51.68	67.26	5.24	55.78	9.39
Mean	78.12	27.83	50.29	64.86	6.95	62.226	11.18